AN EVALUATION OF PARTICLE SIZE MEASUREMENT TECHNIQUES FOR DISPERSED IRON CATALYSTS

V.U.S. Rao
Department of Energy
Pittsburgh Energy Technology Center
P.O.Box 10940
Pittsburgh, PA 15236.

Keywords: Highly dispersed catalysts, Direct coal liquefaction

Abstract

Highly dispersed iron-based catalysts are being examined for the initial stage of direct coal liquefaction. Ultrafine (<10 nm) particles are produced by a variety of methods. Mössbauer spectroscopy, magnetometry, XAFS, electron microscopy, XRD line-broadening, and BET surface area measurement are used to estimate the particle size of the catalyst precursor and, in some instances, of the phases found consequent to the reaction process. With Mössbauer and magnetization techniques, data have to be obtained over a range of temperatures, usually from 4 K to 300 K. In addition, obtaining the particle size by Mössbauer spectroscopy requires a knowledge of the magnetic anisotropy energy. For some XRD lines, the broadening is a consequence of the presence of fault planes rather than crystallite size. The utility of the characterization techniques will be evaluated and comparative results that are available will be presented.

Introduction

The use of inexpensive, ultrafine (<10 nm) iron catalysts for the initial stage of direct coal liquefaction [1] and the conversion of model compounds [2] has attracted attention in recent years. An advantage of using iron is that its disposal after use is not likely to present environmental problems. Hence the development of nanometer-sized, iron-based catalysts could eliminate the need for the expensive catalyst recovery step associated with the more conventional catalysts based on elements such as Mo, Co, Ni and W. Recent studies [1] indicate that ultrafine iron-based catalysts could be active for the first step in coal liquefaction, i.e., solubilization, in concentrations as low as 3,500 ppm with respect to coal.

To support research on the synthesis and testing of iron-based catalysts, it is necessary to have techniques to determine the composition, structural characteristics, and particle size distribution of the catalyst precursor, and more importantly, of the phases during and after the reaction. In the case of iron-based catalysts, the characterization techniques include Mössbauer spectroscopy, magnetometry, XAFS, electron diffraction, XRD, and BET surface area measurement. This paper will attempt to analyze the information that could be obtained from the above techniques and provide comparative results where available.

Phases in Iron-Based Catalysts

It is frequently observed that an iron-based catalyst precursor that is not a sulfide is converted into a sulfided form during coal liquefaction if sufficient sulfur is present in the reaction mixture. The sulfur could be present in coal itself or added as H_2S or S.

A significant fraction of the inorganic sulfur in coal is found as pyrite (FeS_2) which is transformed into pyrrhotite ($Fe_{1-x}S$) under liquefaction conditions according to

$$FeS_2 + (1+x)H_2 \rightarrow Fe_{1-x}S + (1+x)H_2S \quad (1)$$

Depending on the reaction temperature and the partial pressures of H_2 and H_2S, different pyrrhotites characterized by the value of x (typically .07-.12) are observed. The transformation of pyrite to pyrrhotite is slow below 400°C [3].

To investigate the influence of low concentrations of iron-based catalysts, a coal with a minimal quantity of pyrite must be used. For this reason, recent investigations [1] have focussed on the liquefaction of the low-pyrite Blind Canyon coal from Utah [4], which contains only 0.02 wt% pyritic sulfur, compared to 2.1 wt% in Illinois #6 and 0.17 wt% in Wyodak coal.

The approach to attaining ultrafine particle catalysts has been to increase the dispersion of the precursor. Complexes of iron [5], sulfate-promoted oxides [1], and carbides [6] have been used as precursors. In direct liquefaction, in the presence of sufficient sulfur, pyrrhotites are formed, for example [1],

$$Fe_2O_3/SO_4 + S + H_2 \rightarrow Fe_{1-x}S + H_2S + (SO_2, H_2O \text{ etc.}) \quad (2)$$

For compositions ranging between FeS (troilite) and Fe_7S_8 (monoclinic pyrrhotite), the compounds are referred to generally as pyrrhotites [7]. These include Fe_9S_{10}, $Fe_{10}S_{11}$, and $Fe_{11}S_{12}$ which are hexagonal, as is FeS. The hexagonal pyrrhotites are characterized crystallographically by their superstructures of the hexagonal NiAs structure.

It should be mentioned that the above phases are "low-temperature" pyrrhotites. Above 308°C and below its maximum melting point of 1190°C, pyrrhotite exhibits a rather wide homogeneity range as a single solid solution $Fe_{1-x}S$ with the NiAs structure, extending from the stoichiometric FeS to a composition of approximately $Fe_{0.8}S$. Irrespective of the phases found at room temperature in used catalyst samples, it is evident that at liquefaction temperature (350-425°C) the solid solution $Fe_{1-x}S$ is expected. Therefore, *in situ* characterization of the catalyst at reaction condition, although difficult to perform, is desirable.

Mössbauer Relaxation Spectra

The technique of Mössbauer Spectroscopy can be used to detect iron-bearing phases in coal and in liquefaction catalysts [8]. Since the pyrrhotites show magnetic ordering, magnetic hyperfine splitting resulting in a sextet for each magnetically inequivalent Fe site is observed in the Mössbauer spectrum and can be used to identify the phases present [9, 10]. The spectra are frequently

interpreted in terms of three or four inequivalent Fe sites, which have internal magnetic fields in the range 230 to 300 kOe.

In magnetically ordered materials such as the pyrrhotites and Fe_2O_3, one would expect the sextet pattern to broaden and collapse to a quadruple doublet as the particle diameter decreases below a critical diameter, d_c. The corresponding particle volume is designated V_c. Below d_c, the particles exhibit superparamagnetic behavior owing to rapid relaxation of the particle spin system. V_c is given by

$$V_c = kT \ln(f_o/f_L) \; / \; K_a \qquad (3)$$

where K_a is the magnetic anisotropy energy, f_L is the Larmor precession frequency of the ^{57}Fe nucleus, and f_o is a frequency factor which has to be determined for each phase. The particle size distribution can be obtained from an analysis of the Mössbauer relaxation spectra [11].

From an analysis of the Mössbauer relaxation spectra, at temperatures from 10 K to 300 K, of a narrow-size range Fe_2O_3 with the particle diameter centered at 3.2 nm, and using K_a = 0.55 J/m^3 [12], Huffman et al [10] have determined that f_o = 10^{12} s^{-1}. The critical diameter d_c was determined to be 11.8 nm for Fe_2O_3 at 300 K.

Using the above parameters, the particle size range of Fe_2O_3/SO_4 precursors was determined [10] from the observed Mössbauer relaxation spectra. The size distribution showed that nearly 50% of the Fe was in particles that had diameters less than 11.8 nm. The methodology for determining particle size distribution of Fe_2O_3 and related compounds such as FeOOH from Mössbauer relaxation spectra appears to have been established.

In contrast to the above, Mössbauer spectra of pyrrhotites, attributing the unresolved lines to superparamgnetic particles, have been reported in only a few instances [13-15]. Even in these cases, only room temperature spectra were reported; hence the interpretation of the unresolved lines is not unequivocal.

A possible reason for the paucity of confirmed Mössbauer relaxation spectra in pyrrhotites could be the high value of the magnetic anisotropy energy; for example, K_a = 10 J/m^3 for Fe_7S_8 [16,17]. If f_o for Fe_7S_8 is the same as that for Fe_2O_3, one estimates the critical diameter of Fe_7S_8 as being d_c = 4 nm at 300 K. It would appear that the samples that have been examined by Mössbauer spectroscopy do not have pyrrhotite particles whose diameter is less than 4 nm.

Recent progress in the synthesis of fine particles using novel techniques, such as the microemulsion method [18], provides the possibility of synthesizing uniform-size pyrrhotite particles in the 4 nm range. It would then be possible to determine f_o for the pyrrhotites as was done in the case of Fe_2O_3, and use the value of f_o thus derived to estimate the pyrrhotite particle size in liquefaction catalysts.

Magnetometry

In favorable cases particle size distribution can be determined from a measurement of magnetization in a range of applied fields and temperatures [19]. The technique is applicable when the particles in the sample are super-

paramagnetic. In the range of temperatures in which the sample exhibits superparamagnetic behavior, the magnetization is a function of H/T and obeys the Langevin equation:

$$M/M_s = L(M_sVH/kT), \quad L(x) = \coth x - 1/x \tag{4}$$

where M_s and M_s are, respectively, the saturation and spontaneous magnetizations per unit volume, and V is the volume of the particle.

Using a SQUID magnetometer, Ibrahim et al. [19] have determined the particle size distribution of Fe_2O_3/SO_4 samples. A significant fraction of the sample consisted of particles in the 6-10 nm range. The results were in reasonable agreement with the particle size distribution obtained from Mössbauer relaxation spectra. The magnetometric method has not yet been used to determine the particle size of pyrrhotite samples.

XAFS Spectroscopy

Attempts are being made to use XAFS spectroscopy to obtain particle size information on Fe-based catalysts. The analysis of the XAFS spectra provides information on the interatomic distances and coordination numbers of the various neighbor shells to a given Fe atom. Spectra of bulk Fe_2O_3 were compared with those of the fine-particle Fe_2O_3/SO_4 catalyst precursor [10]. While the interatomic distances were similar for the two samples, the average coordination number of the catalyst precursor was significantly lower than that of the bulk sample. This indicated that the Fe atoms in the ultrafine particles that were on or near the surface had, on average, fewer Fe neighbors. Assuming a spherical shape for the particles, particle diameters in the range 1.2-1.8 nm were obtained. The significantly smaller particle diameter obtained using this technique was attributed to the possible nonspherical geometry of the particles.

XRD Line Broadening

The average crystallite dimension of small particles can be estimated from the line broadening of the Bragg peaks using the relation

$$d = 0.9\,\lambda \,/\, B\cos\theta \tag{5}$$

where d = crystallite size, λ = wavelength, B = peak width at half-maximum, and θ is the Bragg angle.

The technique has to be used with caution since faults or other defects can also result in line broadening [20]. Pollack and Spitler [21], who examined pyrrhotites produced in continuous liquefaction units, observed asymmetric Bragg peaks and attributed them to stacking disorder.

Ibrahim et al. [19] examined the XRD line broadening on the same sample of Fe_2O_3/SO_4 on which the Mössbauer and magnetometric studies were performed and found good agreement between the particle size obtained by the different techniques.

Electron Microscopy

Transmission electron microscopy (TEM), in combination with electron microdiffraction, is being employed to examine the particle size distribution and the structural characteristics of iron-based catalysts. In the case of Fe_2O_3/SO_4, the particle size distribution measured by TEM was in agreement with the results from Mössbauer, magnetometry, and XRD line broadening [10].

BET Surface Area

Surface area measurement using the BET method requires a clean surface and is hence limited to the study of catalyst precursors. Pradhan et al. [1] found good correlation between the BET surface area and the average particle size from XRD and TEM on Fe_2O_3/SO_4 samples. In the BET method, nitrogen adsorption at pressures upto 0.1 MPa is frequently used. Lambert et al. [22] have described a more sensitive BET method for measuring the surface area of pyrrhotites using krypton as the adsorbate at -196°C and at pressures from 20 to 270 Pa.

Conclusions

A number of characterization techniques are being successfully used to determine the particle size of iron-based catalyst precursors. In particular, the methods to measure the particle size of Fe_2O_3 and related phases appear to be well established. There is a need to perform additional experimental and theoretical studies to develop methods to measure the particle size of pyrrhotites which seem to be catalytically very important. *In situ* techniques to measure particle size under reaction conditions have to be developed.

Acknowledgements

The author would like to thank M. Farcasiu, S.S. Pollack, G.P. Huffman, F.E. Huggins, K.R.P.M. Rao, B. Ganguly, M.S. Seehra and C.D. Stinespring for helpful discussions.

References

1. See for example, V.R. Pradhan, J.W. Tierney, and I. Wender, ACS Fuel Div. Preprints, **37**, 254 (1992).
2. M. Farcasiu, C. Smith, V.R. Pradhan, and I. Wender, Fuel Process. Tech. **29**, 199 (1991).
3. G.M. Schwab and J.J. Philnis, J. Am. Chem. Soc. **69**, 2588 (1947).
4. Available from the Penn State Coal Research Bank.
5. D.E. Herrick, J.W. Tierney, I. Wender, G.P. Huffman and F.E. Huggins, Energy and Fuels **4**, 231 (1990).
6. F. Derbyshire and T. Hager, ACS Fuel Chemistry Preprints, **37**, 312 (1992).
7. L.F. Power and H.A. Fine, Minerals Sci. Eng. **8**, 106 (1976).
8. See for example, P.A. Montano, Magn. Res. Rev. **7**, 175 (1982).
9. J.C. Ward, Rev. Pure and Appl. Chem. **20**, 175 (1970).
10. G.P. Huffman, B. Ganguly, J. Zhao, K.R.P.M. Rao, N. Shah, Z. Feng, M.M. Taghiei, F. Lu, 1. Wender, V.R. Pradhan, J.W. Tierney, M.S. Seehra, M.M. Ibrahim, J. Shabtai, and E.M. Eyring, Energy and Fuels, in press.
11. V.U.S. Rao, F.E. Huggins and G.P. Huffman, J. Appl. Phys. 50, 2408 (1979).
12. A.M. van der Kraan, Phys. Stat. Sol. (a) **18**, 215 (1973).

13. P. Bussiere, A. Newman and B.K. Sharma, Hyperfine Interactions **42**, 1211 (1988).
14. M. Jamond, R. Bacaud, P.Bussiere, H. Charcosset, and B. Nickel-Pepin-Donat, **52**, 297 (1989).
15. W. Sihao, J. Keyu, W. Zhaoming, G. Jinsheng, W. Youqing, W. Zhen, L. Diwan, Y. Yongquin, and Z. Changgen, Hyperfine Interactions **58**, 2617 (1990).
16. M.J. Besnus, G. Munschy, A.J.P. Meyer, J. Appl. Phys. **39**, 903 (1968).
17. K. Adachi and K. Sato, J. Appl. Phys. **39**, 1343 (1968).
18. See for example, J.C. Linehan, R.M. Beam, D.W. Matson, J.L. Fulton, and A.E. Crump, ACS Fuel Div. Preprints, **37**, 488 (1992).
19. M.M. Ibrahim, J. Zhao, and M.S. Seehra, J. Mater. Res. **7**, 1856 (1992).
20. J.M. Stencel, V.U.S. Rao, J.R. Diehl, K.R. Rhee, A.G. Dhere, and R.J. DeAngelis, J. Catal. **84**, 109 (1983).
21. S.S. Pollack and C.A. Spitler, American Mineralogist 66, 1258 (1981).
22. J.M. Lambert, Jr., P.L. Walker, Jr., A.J. Perrotta, J.P. McCullough and H. Beuther, Fuel **62**, 1474 (1983).

Mössbauer Studies of Fe-Based Ultrafine Coal Liquefaction Catalysts

Bhaswati Ganguly, Frank E. Huggins, K. R. P. M. Rao, and G. P. Huffman
233 Mining and Mineral Resources Building
University of Kentucky
Lexington, Kentucky 40506.

ABSTRACT:

^{57}Fe Mössbauer spectroscopy has been used to investigate a variety of ultrafine iron-based direct coal liquefaction catalysts having either Fe_2O_3 or FeOOH structure. The Mössbauer spectra of these catalysts showed pronounced superparamagnetic effects. The superparamagnetic relaxation spectra were analyzed as a function of temperature using a novel fitting model to determine the particle size distribution for these catalysts[1]. The resulting size distributions are in the nanometer range and agree reasonably well with size information obtained by Scanning Transmission Electron Microscopy (STEM), SQUID magnetometry, and X-Ray Diffraction (XRD).

INTRODUCTION:

In recent years, there has been renewed interest in the use of iron-based catalysts for direct coal liquefaction (DCL)[2-7]. In their as-prepared form prior to liquefaction, such catalysts are normally in the form of highly dispersed iron oxides and oxyhydroxides. The Mössbauer spectra of such fine iron oxide and oxyhydroxide particles exhibit pronounced superparamagnetic relaxation effects, which have been extensively investigated[8-14]. Many of these studies of the superparamagnetic relaxation behavior of small particles have been based on an average particle volume or diameter[8,11-14]. Kundig et al.[9] were the first investigators to describe a method for determining the particle-size distribution of α-Fe_2O_3 by determining the percentage of the Mössbauer spectra in the form of magnetic hyperfine components as a function of temperature. The difficulty with this approach is that Mössbauer spectra are assumed to have sharp transitions from quadrupole doublets to magnetics on lowering the temperature. However, this transition occurs gradually, over a range temperatures. We have used a similar technique to estimate particle size distributions, with a novel model for fitting the Mössbauer spectra that incorporates a superparamagnetic component as well as magnetic hyperfine and quadrupole components.

RESULTS AND DISCUSSIONS:

When particles are small enough to behave superparamagnetically, the rapid relaxation of the particle spin system gives rise to complicated relaxation spectra which are superpositions of broadened magnetic hyperfine spectra, quadrupole doublets, and intermediate superparamagnetic (spm) spectra. Many papers have been written on the dependence of the shape of the Mössbauer spectra on the relaxation time[15-17]. As shown by such authors as Wickman[17], the relaxation time dependent Mössbauer spectrum is given by:

$$I(\omega) = \sum_{i=1}^{6} \frac{K_i[(1+\tau\Gamma_i)P + QR]}{P^2 + Q^2} \qquad (1)$$

where P, Q, R for a zero external magnetic field have the form

$$\begin{aligned} P &= \tau\,[\Gamma_i^2 - (\Delta-\omega)^2 + \delta_i] + \Gamma_i \\ Q &= \tau(\Delta-\omega) \\ R &= (\Delta-\omega)(1+2\tau\Gamma_i) \\ \delta_i &= \frac{1}{2}(\omega_{7-i} - \omega_i), \qquad \Delta = \frac{1}{2}(\omega_{7-i} + \omega_i) \end{aligned} \qquad (2)$$

where τ is the relaxation time in sec, ω is the frequency (in sec^{-1}) corresponding to the Doppler energy of each data point in the Mössbauer spectrum, and ω_i are the frequencies (in sec^{-1}) corresponding to the six allowed transitions between the Zeeman split energy levels. K_i are the Clebsch-Gordon coefficients with $K_6 = K_1 = 3$, $K_5 = K_2 = 2$, and $K_4 = K_3 = 1$ for zero external magnetic field. Γ_i is the natural line width in sec^{-1} and is taken to be the same for all transitions.

A novel method of fitting the spectra is developed, based on the fact that the shape of the Mössbauer spectrum changes with the relaxation time, which in turn can be realated to the size of the particle[1]. Figure 1 shows the theoretical Mössbauer spectra of α-Fe_2O_3 at room temperature as a function of particle-size, derived from Equation 1. It can be seen that at a given temperature, particles with a diameter exceeding some critical diameter, d_M exhibit a magnetic hyperfine spectrum, while particles with a diameter less than some other critical value, d_Q, exhibit a quadrupole doublet. Particles having diameters d such that $d_Q < d < d_M$ exhibit spm relaxation spectra that are neither magnetic nor quadrupole in nature. A typical iron oxide catalyst will normally have a size distribution such that, over some range of temperature, some particles fall into all three size classifications, yielding spectra that are a mixture of magnetic, quadrupole, and spm relaxation spectra. The model consists of fitting the spectra with one or more magnetic hyperfine components corresponding to particles with $d \geq d_M$, one or more quadrupole components, representing particles with $d < d_Q$, and a single spm relaxation spectrum, representing particles for which $d_Q < d < d_M$.

To determine size distributions, the samples are run at several temperatures. The spectrum at each temperature is analyzed using the model mentioned above. The percentage of iron contributing to the magnetic hyperfine component is taken as the percentage of iron contained in particles of volume greater than the critical volume V_c at that temperature. Figure 2 shows a an example of a fit obtained for a sulfated Fe_2O_3 (run at room temperature) using this model, and the size distribution obtained by running this sample at different temperatures. The concept of assigning the percentage of iron contributing to the magnetic hyperfine spectra to particles exceeding a critical volume is similar to the approach of Kundig et al[8]. However, the incorporation of a spm relaxation component enables the magnetic and quadrupole components to be more accurately fit, leading to a correct magnetic percentage, rather than one which artificially incorporates a substantial amount of the spm spectral absorption. A more detailed discussion of this method and its application in determining the size distributions and structures

of a variety of iron-based coal liquefaction catalysts will be published elsewhere[1,18].

SUMMARY:

Mössbauer spectroscopy has been used to derive the size dispersion of a variety of ultrafine iron based direct coal liquefaction catalysts which show superparamagnetic behavior. A novel method of fitting the spectra was developed, in which the larger particles were represented by magnetic hyperfine components, the smaller particles by quadrupole doublets, and particles of intermediate volume by a spm relaxation spectrum. The size distributions were determined by measuring the magnetic hyperfine percentage as a function of temperature, each temperature corresponding to a critical diameter required for a magnetic Mössbauer spectrum. Comparison of the size distributions determined in this manner to size information obtained from TEM, SQUID magnetometry and XRD gave reasonable agreement[1]. The advantage of this fitting model is that it does not assume any kind of standard distribution, but numerically fits the data itself as a combination of magnetic, quadrupole and spm component. Moreover, it is possible to obtain a rough estimate of the size distribution from a spectrum obtained at a single temperature, provided the spectrum exhibits a reasonable amount of all three spectral components (magnetic, quadrupole, and spm).

ACKNOWLEDGEMENTS:

This research was supported by the U.S. Department of Energy under DoE contract No. DE-FC22-90-PC90029, as part of the research program of the Consortium for Fossil Fuel Liquefaction Science. We are grateful to Bernard M. Kosowski of Mach I, Inc., for providing the sample used in this research.

REFERENCES:

1. Ganguly, B., Hugging, F.E., Rao, K.R.P.M., and Huffman, G.P; "Determination of the Size of Iron Oxide Catalysts from Superparamagnetic Mössbauer Relaxation Spectra"; submitted to the Journal of Catalysis.
2. Suzuki, T.; Yamada,O; Takehashi, Y.; Watanabe, Y., Fuel Process Technol., 1985, 10, 33.
3. Tanabe, K.; Yamaguchi, T.; Hattori, H.; Sanada, Y.; Yokoyama, S., Fuel Process. Technol., 1984, 8, 117.
4. Herrick, D.E.; Tierney, J.W.; Wender, I.; Huffman, G.P.; and Huggins, F.E., Energy & Fuels, 1991, 4, 231.
5. Pradhan, V.R.; Tierney, J.W.; Wender, I.; Huffman, G.P.; Energy & Fuels, 1991, 5, 497.
6. Cook, P.S.; Cashion, J.D., Fuel, 1987, 66, 661.
7. Huffman, G.P.; Huggins, F.E.; Ganguly, B.; Shah, N.; Taghiei, M.M.; Hager, G.T., Proceedings, 1991 International Conference on Coal Science, Newcastle, England, Ed. Int. Energy Agency, Butterworth-Heineman Ltd., 1991, 826.
8. Shinjo, Teruya, J. Phys. Soc. Jap., 1966, 21(5), 917.
9. Kundig,W., Bommel, H., Constabaris, G., Lindquist, R.H., Phys Rev., 1966, 142, 327.
10. Van der Kraan, A.M., Phys. Stat. Sol. (a), 1973, 18, 215.

11. Vertes, A., Huang, T.C., Van der Hoff, J.W., Lazar, K., Bennetech, M., Reiff, W., Radiochem. Radioanal. Lett., 1983, 59(5-6), 307.

12. Van der Kraan, A.M., Thesis (1972).
13. Rodmacq, B., J. Phys. Chem. Solids, 1984, 45(11-12), 1119.
14. Roggwiller, P.; Kundig, W., Sol. State Comm., 1973, 12, 901.
15. Van der Woude, and Dekker, A.J., Phys. Stat. Sol., 1966, 13, 181.
16. Blume, M., and Tjon, J.A., Phys. Rev., 1968, 165, 446.
17. Wickman, H.H., "Mössbauer Effect Methodology", Vol II (ed. I.J. Gruverman), 1966, pp 39, Plenum Press, NY.
18. Huffman, G.P., et al.; "Structure and Dispersion of Iron-Based Catalysts for Direct Coal Liquefaction"; Energy and Fuels, in press.

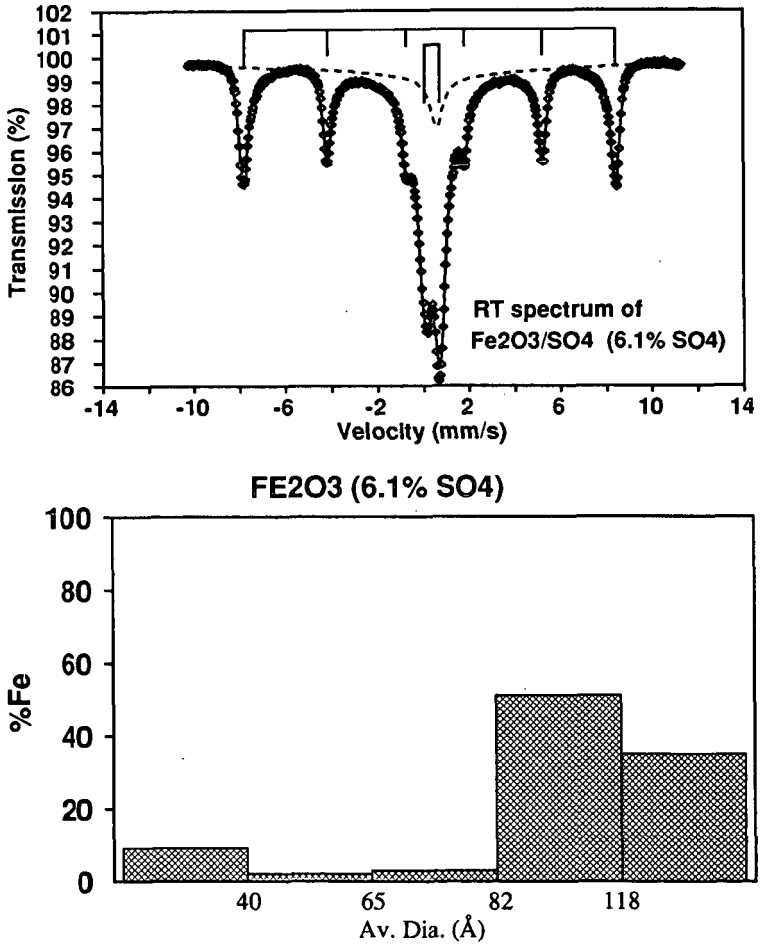

Figure 2. An example of a superparamagnetic fit and the size distribution obtained by running the sample at several temperatures.

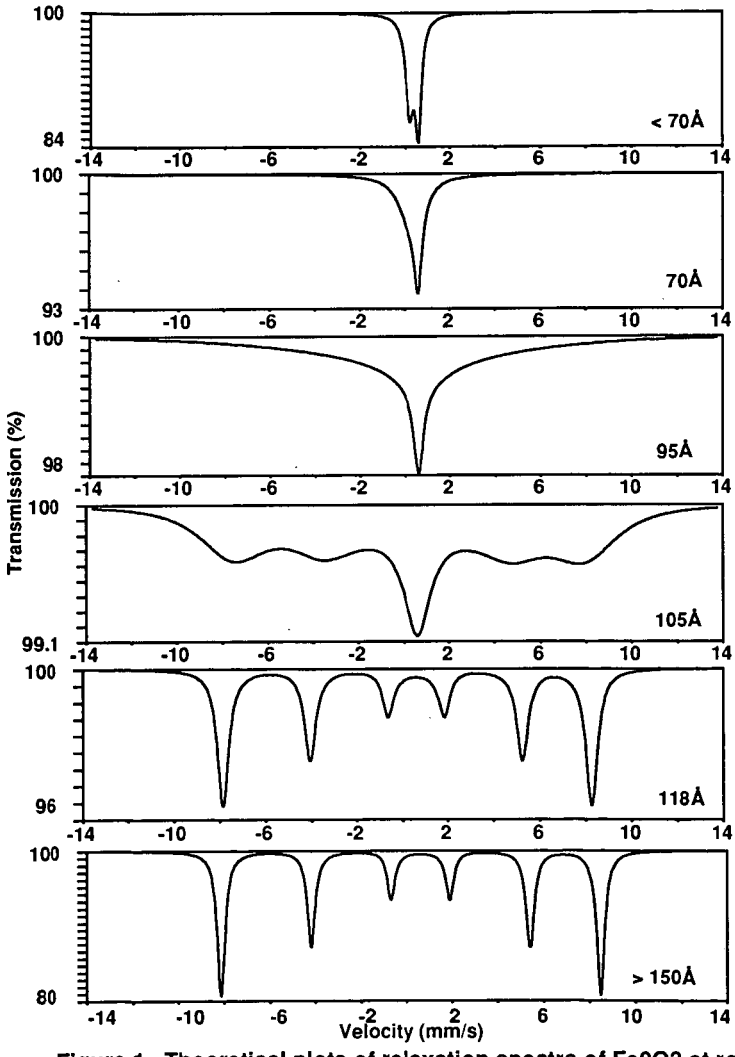

Figure 1. Theoretical plots of relaxation spectra of Fe2O3 at room-temperature as a function of particle size.

STRUCTURE AND PHASE TRANSITION OF AN ULTRAFINE IRON OXIDE CATALYST

J. Zhao, Z. Feng, F. E. Huggins, N. Shah and G. P. Huffman*
233 Mining and Mineral Research Building
University of Kentucky
Lexington, KY 40506

I. Abstract

The structure and phase transitions of an iron oxide catalyst with average particle diameter of 30Å have been examined by means of X-ray absorption fine structure (XAFS) spectroscopy, thermal gravimetric analysis (TGA), Mossbauer spectroscopy, and transmission electron microscopy (TEM). The structure is found to be an FeOOH with surface iron ions at coordination unsaturated (CUS) sites or Lewis acid sites. At annealing temperatures of 250 to 350°C, the sample only partly converts to larger α-Fe_2O_3 particles. The conversion rate is greatly accelerated if the sample is exposed in air for several days. The results indicate that the 30Å particles become linked by water molecules adsorbed at the CUS sites after air exposure. At elevated temperature, these water molecules are evolved from between the particles, facilitating both agglomeration of the particles and phase transition to α-Fe_2O_3.

II. INTRODUCTION

In recent years, significant efforts have been made to produce highly dispersed iron catalysts for direct coal liquefaction (DCL), in order to increase surface area and minimize catalyst loading. Improved dispersion and conversion rate have been obtained by modifying the surface structure by adding small amount of sulfur and other elements to the catalyst [1]. Studies have shown that, at the sulfated iron oxide (Fe_2O_3/SO_4) surface, coordination unsaturated (CUS) sites or Lewis acid sites are formed [2]. It has been suggested that a sulfated surface may prevent agglomeration of small catalyst particles during reaction [1]. The activity is also found to be sensitive to the surface conditions as determined by the moisture content of the catalysts [1,3]. These observation indicate that the surface structure and surface conditions are crucial for catalyst performance, although the exact mechanisms are still unclear.

II. EXPERIMENTAL

The catalyst sample (NANOCAT™) is manufactured by Mach I., Inc. In addition to the as-received sample, several samples were prepared by annealing the as-received sample in air for 24 hrs at temperatures from 250 to 500°C. To observe the effect of moisture, part of the as-received sample was first exposed in air for five days at room temperature, and subsequently annealed at 250°C in air for 24 hrs.

X-ray absorption spectra were collected at the National Synchrotron Light Source (NSLS) on beam line X-19A at Brookhaven National Laboratory. All spectra were collected in the transmission mode and at liquid-nitrogen temperature.

Transmission electron micrographs and micro-diffraction patterns were obtained with a Hitachi H800 NA microscope. The operating voltage was set at 200kV for all samples.

Mössbauer spectra were recorded with a constant acceleration spectrometer. The

radioactive source consists of ~50 mCi of ^{57}Co in Pd matrix. Spectra were recorded at 10 K with an Air Products displex cryogenic system.

Thermogravimetric analysis (TGA) were performed with a Seiko 320 TGA/DSC system.

III. RESULTS

Structure of the 30Å Catalyst

The EXAFS radial structure functions (RSF) of the 30Å catalyst and several iron oxides and oxyhydroxides are shown in Figure 1. The position of the first Fe shell is close to that for oxyhydroxides. Least squares fitting for the 30Å catalyst gives first Fe coordination shell at 3.01 Å. By comparing with the first Fe shell distances of iron oxides (2.92-2.95 Å) and iron oxyhydroxides (3.01-3.05 Å), we conclude that the structure of the 30Å catalyst is oxyhydroxide (FeOOH) like. The x-ray absorption near edge structure (XANES) for the 30Å catalyst is also similar to that for the oxyhydroxides.

Although both EXAFS and XANES for the 30Å catalyst indicates an FeOOH structure in which iron ions are coordinated by total six oxygens or hydroxyl groups, the intensity of pre-edge structure (Figure 2) of the catalyst is 1.7 times that for those octahedral oxides and oxyhydroxides, indicating that part of the iron ions have coordination less that six [4]. After an extended period of exposure of the sample to air, the average coordination number is increased as indicated by the decrease of the pre-edge peak. Therefore, these low coordination sites are likely to be at the particle surface. These sites, created by dehydroxylation on the oxide surface, are also known as CUS (coordination unsaturated) sites or Lewis acid sites. More details of the structure analysis are given in Ref. 5.

Effect of Annealing

The TGA curve for the fresh 30Å catalyst is compared to that of α-FeOOH in Figure 3. At temperatures < 300°C, α-FeOOH converts to α-Fe_2O_3 by releasing H_2O, resulting in 11% weight loss. For α-FeOOH, the phase transition occurs between 200 to 270°C, as shown in the figure. For the 30Å catalyst, although a ~12% weight loss at T > 700°C suggests that the above reaction does occur, no clear phase change was observed from room temperature up to 900°C.

TEM micrograph of the sample after 250°C annealing for 24 hrs indicates the coexistence of two phases (Figure 4a); the small particle 30Å FeOOH phase and a larger particle (d≈150Å) α-Fe_2O_3 phase. The volume fraction and average particle size of the larger α-Fe_2O_3 particles increases with annealing temperature. However, a considerable percentage of the 30Å particles appears to be unchanged even after 24 hrs annealing at temperatures up to 350°C which would completely convert α-FeOOH to α-Fe_2O_3. At annealing temperatures of 400°C and higher, larger particles dominates and the particle size becomes uniform. The phase transition rate is greatly accelerated if the 30Å catalyst is exposed to moist air before annealing. After annealing at 250°C in air for 24 hrs, the moisture exposed sample mainly consists of larger particles with diameters of ~150Å, as shown in TEM micrographs (Figure 4b).

The percentages of the two iron phases in the annealed samples are determined by Mossbauer spectroscopy [6]. After annealing at identical conditions, the as-received sample consists of 65% 30Å FeOOH phase and 34% α-Fe_2O_3 phase, whereas the air-exposed sample consists of 26% 30Å FeOOH phase and 73% α-Fe_2O_3 phase.

IV. DISCUSSION

The difference of phase transition rates between the as-received and air exposed 30Å

FeOOH catalysts at elevated temperature is attributed to their surface conditions.. A surface layer with CUS sites can effectively prevent not only the agglomeration of the small 30Å FeOOH particles, but also dehydroxylation in the sample bulk, thereby slowing down the phase transition. However, after moisture exposure, the small 30Å particles become linked by adsorbed H_2O molecules on the surface. At elevated temperature, these water molecules are evolved from the particle joints, leading to agglomeration and phase transition to α-Fe_2O_3. A diagram of this process is shown in Figure 5. It appears that the phase transition to α-Fe_2O_3 occurs immediately after the agglomeration takes place, as indicated by the TEM and Mössbauer results, which show no trace of larger FeOOH particles. At annealing temperatures below 350°C, the rate of phase transition is determined mainly by the coverage of the water molecules adsorbed on the particle surface. Agglomeration and phase transition take place mainly in those particles linked by water molecules. At T > 350°C, the transition to α-Fe_2O_3 is due to the dehydroxylation inside of the 30Å catalyst particle. It should be noted that only those H_2O molecules adsorbed on the CUS sites may remain on the particle surface at T > 250°C or higher. Physisorbed H_2O molecules, since the their bonding to the particle surface is much weak, will be detached from the particle surface at temperature well below 250°C.

Acknowledgement

The support of the U.S. Department of Energy for this research under contract No. DE-FC22-90029 is gratefully acknowledged. This investigation was carried out as part of the cooperative research program of the Consortium for Fossil Fuel Liquefaction Science.

We would also like to acknowledge Dr. Aurora Rubel and Mr. Larry Rice, both at University of Kentucky, for their assistance with the TGA and TEM measurements.

References

1. Pradhan, V. R.; Tierney, J. W.; Wender, I., and Huffman, G. P., *Energy & Fuels*, **5**, 497 (1991).
2. Jin, Tuo; Yamaguchi, Y.; Tanabe, K., *J. Phys. Chem.* **90**, 4795 (1986).
3. Farcasiu, M., unpublished results.
4. Roe, A. L., et al., *J. Am. Chem. Soc.* **106**, 1676 (1984).
5. Zhao, J.; Huggins, F.E.; Feng, Z.; Lu, F.; Shah; N.; and Huffman, G. P.; to be published.
6. Feng, Zhen; Zhao, J.; Huggins, F.E.; and Huffman, G.P. to be published.

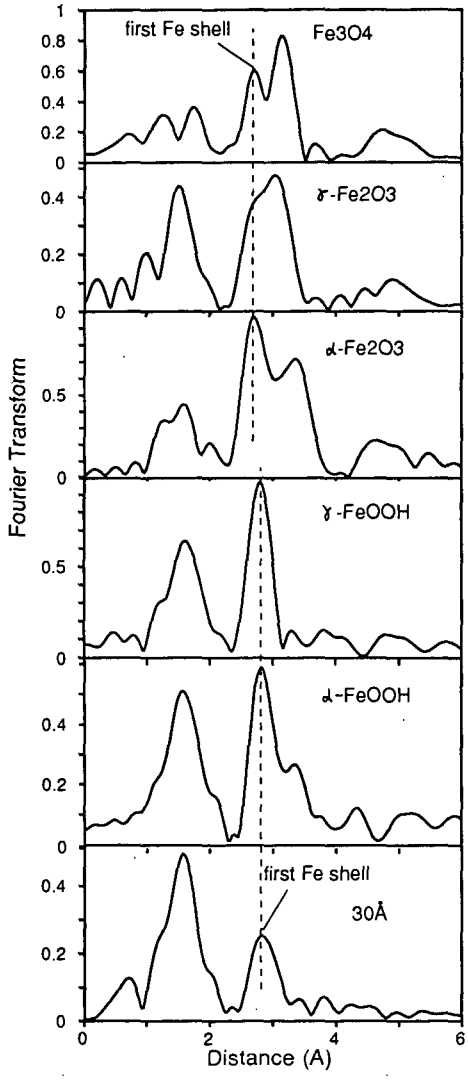

Figure 1. EXAFS RSF's for the 30Å catalyst and model compounds.

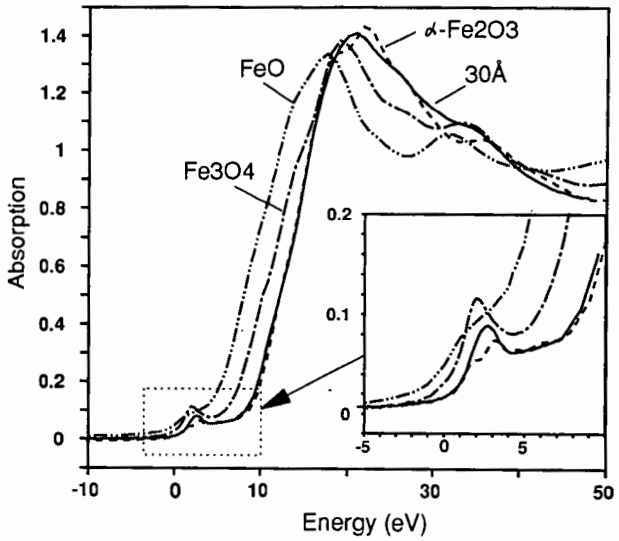

Figure 2. XANES pre-edge structures of the 30Å catalyst and model compounds.

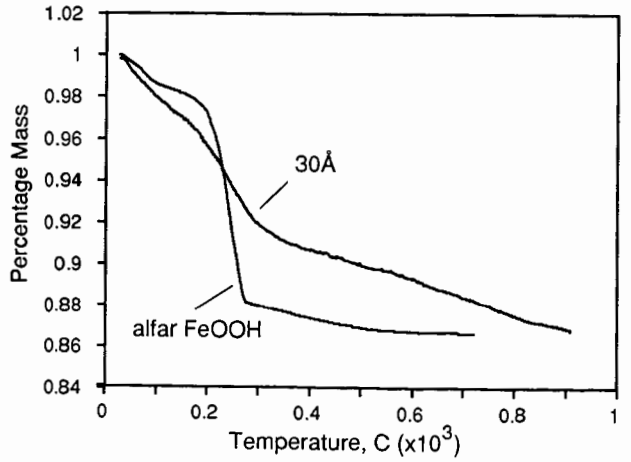

Figure 3. Thermogravimetric analysis for α-FeOOH and the 30Å catalyst.

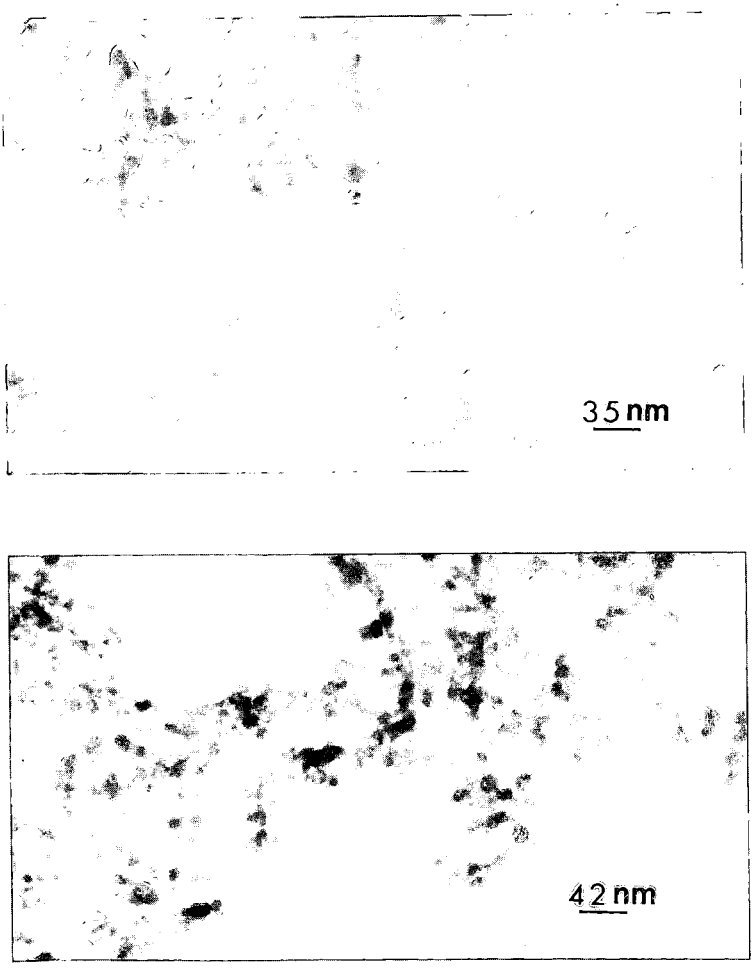

Figure 4. TEM micrographs of the as-received 30Å catalyst (top) and moist air exposed 30Å catalysts (bottom), after annealed at 250C for 24hrs.

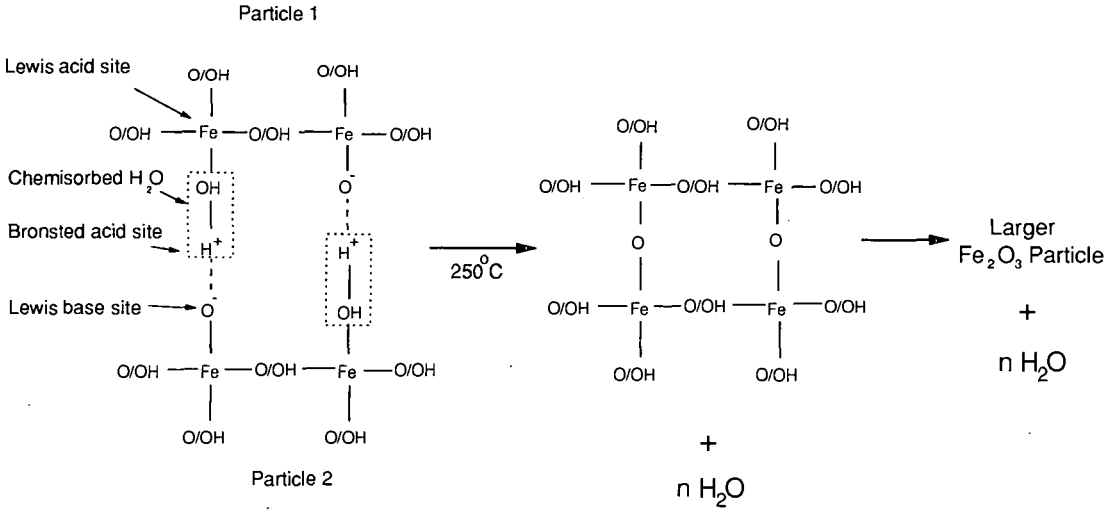

Figure 5. Proposed scheme of agglomeration and phase transition of the 30Å catalyst.

CHARACTERIZATION OF SULFIDED IRON CATALYSTS

Ram Srinivasan, Robert A. Keogh, and
Burtron H. Davis

Center for Applied Energy Research
University of Kentucky
3572 Iron Works Pike
Lexington, KY 40511

ABSTRACT

An ultrafine iron oxide and a FeOOH sample were sulfided using a H_2S/N_2 mixture at room temperature. The sulfided samples obtained at room temperature were also run in a microautoclave reactor using a temperature of 200°C for 30 min. using a H_2S/H_2 atmosphere and tetralin as a solvent. The sulfided iron catalysts were characterized by TEM and EDAX.

INTRODUCTION

Coal liquefaction can be accomplished by thermolysis; however, it was quickly realized that improved yields could be obtained through the use of catalyst (1). One of the first catalysts studied was an iron oxide in one of several forms (1-3) and is still widely used today (4).

Initial coal liquefaction products may have very high molecular weights. These initial dissolution products are so large that they will not be able to diffuse into the smaller pores of most heterogeneous catalysts. It is therefore desirable that catalysts, especially those used in the reactor which involve the initial dissolution reactions, have the active component on the geometric surface of the catalyst particle. It is also desirable that these catalysts have a high surface area in order to obtain a high rate of conversion. These two factors indicate that the desirable catalyst will be one which is comprised of colloidal or smaller nonporous individual particles.

Although a large volume of work has been carried out to determine product yield, reaction conditions, etc., very limited work has been available in terms of microscopic characterization of catalyst powders. The results presented in this work used an ultrafine γ-Fe_2O_3 (S.A. = 270 m^2/g) and an γ-FeOOH precursor which have been sulfided at room temperature and at higher temperatures. The characterization of these catalysts are presented.

EXPERIMENTAL

The γ-Fe_2O_3 and γ-FeOOH were hydrated in a chamber saturated with H_2O prior to sulfidation. Both catalyst precursors showed approximately a 28 wt.% gain in 48 hours. The dry samples could not be sulfided at room temperature. The catalyst precursors were sulfided using 5 mole % H_2S in nitrogen. Approximately 2g of the hydrated precursors were placed in a flask containing ca. 20g of tetralin and the H_2S/N_2 mixture was bubbled through the catalyst/tetralin slurry. The resulting sulfided samples were stored in the flask under the H_2S/N_2 atmosphere prior to running at 200°C in the batch autoclave and

analysis. Aliquots of the sulfided catalysts/tetralin slurry were transferred to a 25cc microautoclave reactor. The reactor was pressurized to 800 psig (ambient) with a 10% H_2S in H_2 and placed in a fluidized sand bath. The reaction was run at 200°C for 30 min.

The samples for electron transmission microscopy (TEM) analysis were prepared in the glovebox in flowing nitrogen. A few drops of the sample were transferred to a 100 cc beaker and washed with ethanol twice, and then ultrasonically agitated in ethanol. A drop of this suspension was placed on a carbon coated 200 mesh copper grids. Ethanol evaporated leaving a thin film of particles on the grids. These TEM grids were then transferred to a vacuum desiccator until they were inserted into the microscope. While transferring the samples into the microscope the samples were exposed to the atmosphere less than a minute.

For TEM analysis, a Hitachi H800 NA scanning microscope was used at 200 kV. Microdiffraction and energy-dispersive X-ray (EDX) analyses were carried out in a nanoprobe mode (5 nm). This implies that the microdiffraction and EDX data obtained were from a 5 nm regions of the sample. This microscope is equipped with a silicon-lithium diode detector (Link) and a multi-channel analyzer (Tracor 500). The X-rays emitted by the specimen were collected in the range 0-20 KeV for 60 seconds.

RESULTS AND DISCUSSION

Room Temperature Sulfidation of γ-FeOOH

Many agglomerated large "blobs" were seen for this sample. Microdiffraction patterns could not be obtained from these blobs. A typical electron micrograph is presented in Figure 1. EDX from these blobs yielded very strong FeKα and SKα lines. These large blobs easily disintegrated under the beam giving rise to a good dispersion of small hexagonal particles. A representative micrograph from such a dispersed area of the sample is presented in Figure 2. EDX from these particles showed only FeKα, and these individual particles yielded microdiffraction patterns.

γ-FeOOH Sulfidation at 200°C

Contrary to the results of the above sample at room temperature, this sample contains large, thin hexagonal iron sulfide crystals. A typical micrograph of this sample is presented in Figure 3. EDX analysis of the large hexagonal crystals yielded strong signals for both FeKα and SKα lines. A typical electron microdiffraction pattern obtained from one such crystal is presented in Figure 4. This microdiffraction patterns indicates that the crystal is Fe_7S_8 in $[001]_{hcp}$ orientation. Microdiffraction patterns and EDX data from several hexagonal particles consistently proved that these large hexagonal crystals are Fe_7S_8.

Room Temperature Sulfidation of γ-Fe_2O_3

This sample contains regions of free sulfur and needle-shaped α-Fe_2O_3. A region containing long needles of α-Fe_2O_3 is shown in Figure 5. Electron microdiffraction pattern obtained from these particles indicated that these sticks are α-Fe_2O_3. EDX data from these needles showed only FeKα. A typical region containing free sulfur in the form of flowers is shown in Figure 6. EDX from this region showed only sulfur. Also, regions containing hexagonal dense sulfur particles were evident as shown in Figure 7. No evidence for iron sulfide particles was obtained. Consequently, it appears that the α-Fe_2O_3 converts H_2S to

S plus H_2, more likely, that the sulfide formed is oxidized during the brief exposure to air during sample transfer.

γ-Fe_2O_3 Sulfidation at 200°C

This sample contained regions of both long, rectangular particles and the large hexagonal particles. As before, the large, thin hexagonal particles were found to be Fe_7S_8 crystals both by electron microdiffraction and EDX analyses. A bright field electron micrograph (Figure 8) shows the presence of both these two kinds of particles. A typical electron microdiffraction pattern obtained from one of the large hexagonal crystals is presented in Figure 9, which is $[001]_{hcp}$ orientation. No free sulfur could be identified as was the case for the sample sulfided at room temperature.

ACKNOWLEDGMENT

This work was supported by the Commonwealth of Kentucky and DOE Contract No. DE-FC22-88PC8806 as part of the Consortium for Fossil Fuel Liquefaction Science (administered by the University of Kentucky).

REFERENCES

1. Bergius, F., "Chemical Reaction Under High Pressure", Nobel Lecture, May 21, 1932.
2. Stranges, A. N., *Fuel Proc. Tech.*, **1987**, 16, 205.
3. Wu, W. R. K.; Storch, H. H., "Hydrogenation of Coal and Tar", Bulletin 683, Bureau of Mines, U.S. Department of Interior, Washington, DC, 1968.
4. Lee, J. M.; Cantrell, C. E.; Gollakota, S. V.; Davies, O. L.; Corser, M. M.; Vimalchand, P., *ACS Div. Fuel Chem. Preprints*, **1991**, 36, 1915.

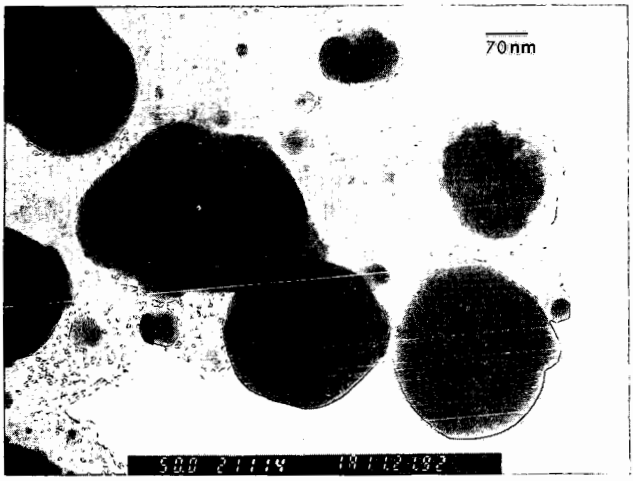

Figure 1. Typical micrograph of the "blobs" from the room temperature sulfidation of γ-FeOOH.

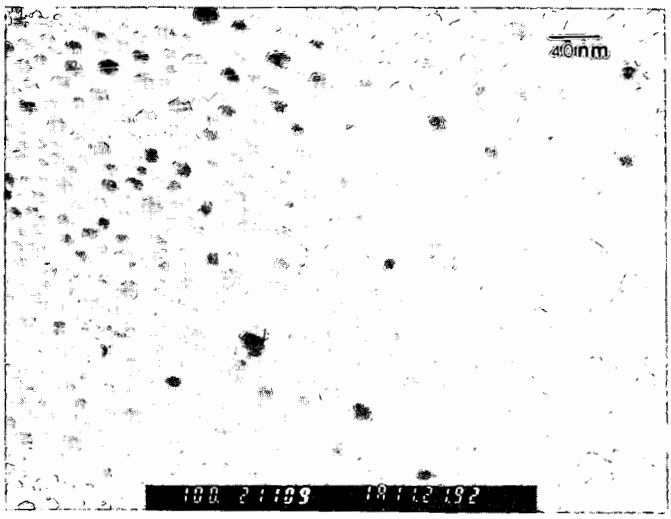

Figure 2. Micrograph of the disintegrated "blobs" using the electron beam.

Figure 3. Microcgraph of the particles from the sulfidation of γ-FeOOH at 200°C.

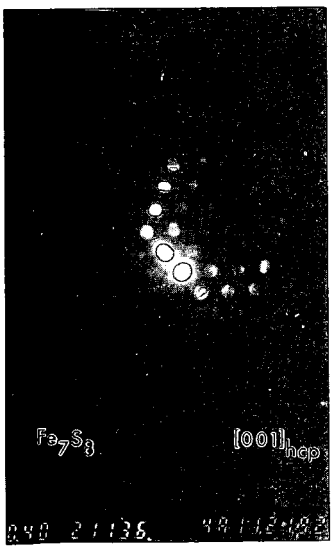

Figure 4. Microdiffraction pattern of the sulfided γ-FeOOH at 200°C.

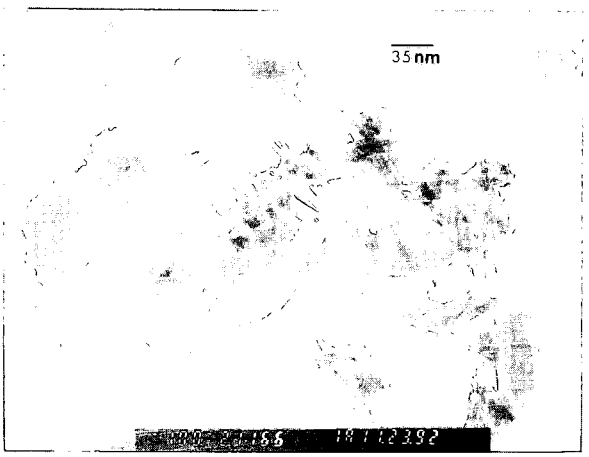

Figure 5. Micrograph of the particles from the room temperature sulfidation of γ-Fe_2O_3.

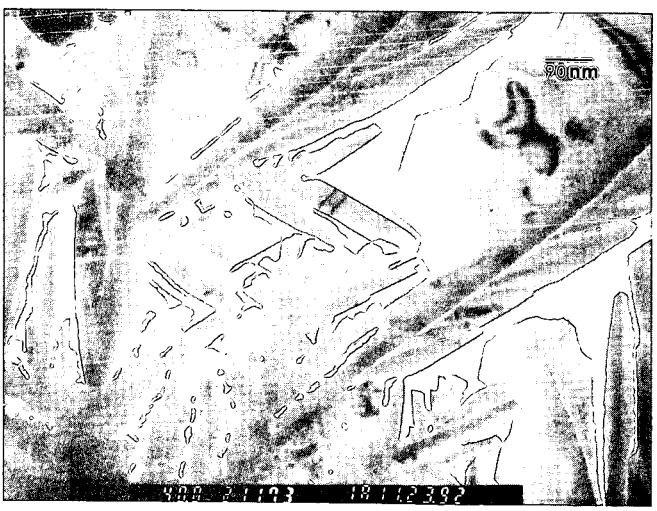

Figure 6. Micrograph of the region containing free sulfur from the room temperature sulfidation of γ-Fe_2O_3.

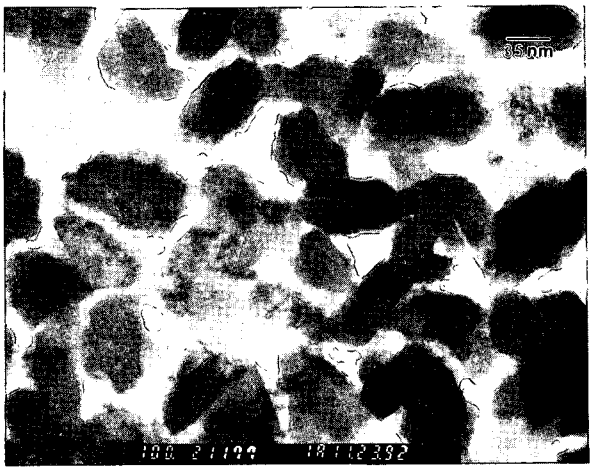

Figure 7. Micrograph of the region containing hexagonal sulfur from the room temperature sulfidation of γ-Fe_2O_3.

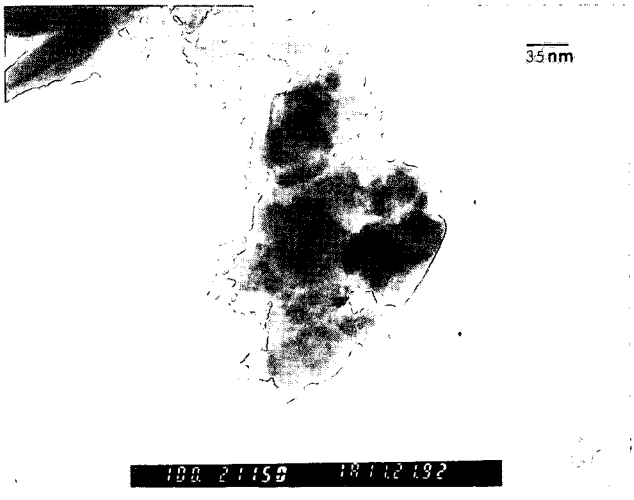

Figure 8. A bright field electron micrograph of the γ-Fe_2O_3 sample sulfided at 200°C.

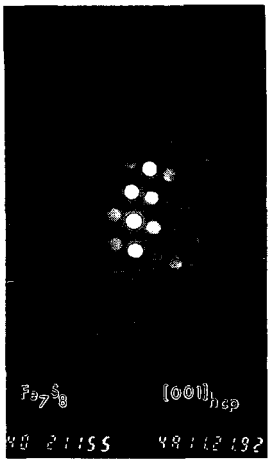

Figure 9. Microdiffraction pattern from the large hexagonal particles (γ-Fe_2O_3) sulfidation at 200°C.

TRACKING IRON CATALYSTS IN HYDROTREATED BLIND CANYON COAL

David A. Sommerfeld, Wisanu Tuntawiroon, Larry L. Anderson and Edward M. Eyring, Department of Chemistry and Department of Chemical and Fuels Engineering, University of Utah, Salt Lake City, UT 84112

Introduction

In the past several years we have researched the dispersion of iron based catalysts within coal and coal macerals. This work has focussed not only upon the dispersion itself, but also upon the effect of the catalyst dispersion on the efficiency of the coal liquefaction process.

In experiments done with vitrinite and resinite macerals derived from Hiawatha (Utah) coal we found that an acetone soluble iron catalyst is more readily dispersed within the vitrinite than within the resinite maceral.[1] Using petrographic, IR spectroscopy and thermogravimetric analysis of the products, we determined that the vitrinite macerals had undergone a greater degree of depolymerization than the resinite maceral. In fact, the degree of aromaticity had increased in the resinite maceral indicating an overall loss of hydrogen during the hydrotreatment process. This retrograde process in the resinite maceral was attributed to the incomplete dispersion of the iron catalyst throughout this maceral.[1]

Further research with a suite of coals from the Argonne Premium Coal Sample Program indicated that the C, H, O elemental composition of the coal plays an important role in the catalyst dispersion and the efficiency of the liquefaction process.[2] It was

found that Wyodak, a low rank coal, gave a significantly greater yield of tetrahydrofuran (THF) solubles than does Pittsburgh #8, a higher rank coal. This result was attributed, in part, to the oxygen content of the coals. Wyodak coal has more oxygen, and this permits a greater degree of cross linking to occur during the hydrotreatment process. Cross linking preserves the pore structure of the coal thus facilitating the movement of the catalyst into the interior of the coal particle. In Pittsburgh #8, with a lower oxygen content than Wyodak coal, less cross linking occurs during hydrotreatment resulting in a poorer dispersion of the catalyst and a lower yield of THF solubles.[3]

In the past year we have been working with different forms of iron based coal liquefaction catalysts. The present paper covers some of our latest results that involve a comparison of catalyst efficiency and dispersion for various iron based catalysts with Blind Canyon (Utah) coal (DECS-17 from the Penn State Coal Sample Bank).

Experimental

The results reported in the present preprint were obtained using sealed glass tube reactors. Each reactor vessel contained 200 mg of catalyst impregnated DECS-17 coal and 400 mg of 9,10-dihydrophenanthrene which served as the hydrogen donor for the experiment. The catalyst loading for these experiments was 1 wt% by iron (and 1 wt% Mo or W in the case of the bimetallic catalyst systems). The sealed reaction vessels were then heated at 350°C for one hour. The THF solubles were obtained via soxhlet

extraction.

Catalysts were prepared in the following manner: If the catalyst was a dry, insoluble powder, the coal and catalyst were simply mixed together. Some coal samples were impregnated with catalysts derived from water soluble salts by an incipient wetness technique. The Mach 1 iron oxide catalyst was obtained from the Mach 1 Corporation (King of Prussia, PA). Presulfided Mach 1 was prepared in the following manner: 1 g of Mach 1 was placed in a tube oven. H_2S gas (1 atm) was allowed to saturate the sample, which was then heated to 400°C for two hours; the Mach 1 powder turned black. Upon exposure to air the catalyst underwent combustion and returned to a rust color.

The degree of dispersion of the catalyst systems was determined by making electron probe microanalysis (EPMA) micrographs of the THF insoluble fraction of the product. EPMA is a technique which allows one to map the dispersion of a given chemical element within a sample by the detection of characteristic X-rays.[4] The coal samples were mounted in Petropoxy 154 and polished to the required smoothness on a Syntron diamond paste polisher. Visual images were obtained using both secondary electron images (SEM) and back-scattered electron images (BSE). EPMA micrographs were obtained for iron and sulfur, and when necessary for molybdenum and tungsten.

The glass tube studies reported here will be repeated using a shaken, horizontal, tubing bomb reactor. These tubing bomb reactions will be done at 350°C for one hour and 2000 psig H_2. THF solubles yields and EPMA micrographs will be obtained.

Results

The present results are for the glass tube experiments. Data from the tubing bomb reactions will be presented at the Denver meeting.

EPMA micrographs for raw, hydrotreated DECS-17 coal show very little background iron and no molybdenum. The expected sulfur background is seen evenly dispersed throughout the particle. The images obtained for the iron/molybdenum bimetallic, soluble salt derived catalyst exhibit the following pattern: The iron has fully penetrated the coal particle and maps onto the sulfur; the molybdenum has also entered the coal particle. To some extent the molybdenum has collected in two void spaces within the particle (Figures 1a and 1b). The EPMA micrographs of the iron/thiotungstate impregnated sample tell a different story. In this case the iron generally remains outside the coal particle (Figure 2a). The sulfur and tungsten EPMA micrographs map onto each other very nicely, but neither sulfur nor tungsten has fully penetrated the coal particle. Instead, the thiotungstate remains near the exterior of the coal particle forming a halo (Figure 2b).

Two other samples were examined using EPMA. Both of these samples involved catalysts that are made of finely granulated iron oxide powders: Mach 1 and an Fe_2O_3/MoO_4 catalyst from the laboratory of Dr. Irving Wender (University of Pittsburgh). In the case of the presulfided Mach 1 catalyst the iron does not enter the coal particle. The iron and sulfur map onto each other indicating that some sulfur remains present even after the combustion process that

the catalyst underwent after presulfidation. The iron remains clumped together, a feature which was seen in samples treated with unsulfided Mach 1 (Figure 3). No molybdenum was added, and no molybdenum was found in the EPMA micrographs. According to EPMA micrographs (not shown), the catalyst provided by Irving Wender also did not enter the coal during hydrotreatment. The EPMA micrographs of the coal (not the catalyst) particles show typical native sulfur and iron backgrounds and no trace of molybdenum.

Due to the inherent uncertainties associated with the use of sealed glass tubes (i.e., loss of gaseous products and incomplete collection of the solid product), we do not report any THF solubles yields in this preprint. THF solubles yields will be reported at the Denver meeting for the reactions conducted in the tubing bomb reactors.

Conclusions

Water soluble salts are the most completely dispersed catalysts in the coal particles. In the case of the iron/molybdenum combination, the metallic species have fully penetrated the coal particle. Even though Mach 1 exists as a very fine particulate (average diameter 30 Å) it does not enter the coal particle. If the efficiency of the coal liquefaction process depends upon catalyst dispersion then soluble catalysts introduced by the incipient wetness technique have a significant advantage over insoluble, particulate based catalyst systems.

Acknowledgements

We would like to thank Dr. Irving Wender for samples of the Fe_2O_3/MoO_4 catalyst and Ray Lambert for valuable technical assistance. Funding was provided by the Department of Energy Fossil Fuels Division through the Consortium for Fossil Fuel Liquefaction Sciences Contract No. UKRF-4-21003-86-24 (DE-FC22-89PC89851).

References

1. H.P. Wang, R. Lo, D.A. Sommerfeld, H. Huai, R.J. Pugmire, J. Shabtai and E.M. Eyring, "Spectroscopic Studies of Coal Maceral Depolymerization Effected by an Iron-Based Catalyst," **Fuel**, 71, 723 (1992).

2. D.A. Sommerfeld, J. Jaturapitpornsakul, L.L. Anderson and E.M. Eyring, "Microscopic Studies on the Dispersion of Iron/Molybdenum Bimetallic Catalysts in Argonne Coals," (submitted to **Fuel Processing Technology**).

3. F. Derbyshire, "Vitrinite Structure: Alterations with Rank and Processing," **Fuel**, 70, 276, (1991).

4. D.E. Newbury, C.E. Flori, R.B. Marinenko, R.L. Myklebust, C.R. Swyt and D.S. Bright, "Compositional Mapping with the Electron Probe Microanalyzer: Part I," **Anal. Chem.**, 62, 1159A, (1990).

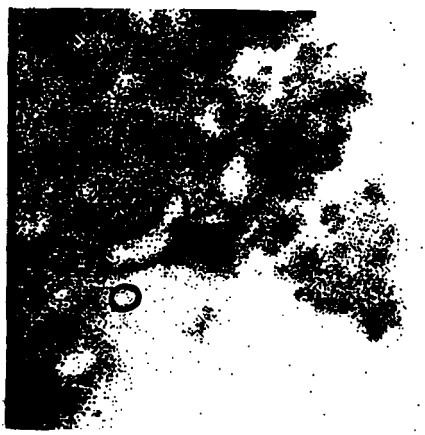

Figure 1a. This EPMA micrograph is 45μm by 45μm. The coal particle occupies the left and center of the image. Iron is well dispersed throughout this region. Note two void spaces circled in the figure.

Figure 1b. The EPMA micrograph is 45μm by 45μm and maps the Mo content of the coal particle. The coal particle occupies the left and center of the image. The Mo is well dispersed throughout the particle with two regions of greater concentration (circled) occurring in void spaces of the particle.

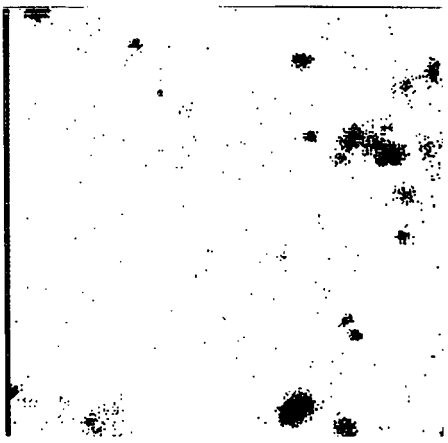

Figure 2a. The EPMA micrograph is 45μm by 45μm and represents the iron distribution in the coal particle. In this image the coal particle occupies the top and center. Only a small area has been penetrated by iron along the right side of the particle.

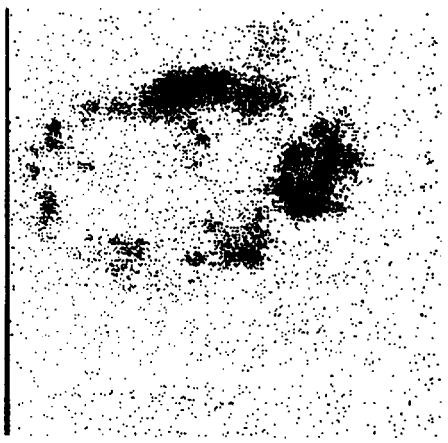

Figure 2b. The EPMA micrograph is 45μm by 45μm and represents the tungsten distribution within the coal particle. The tungsten has not fully penetrated the particle. Instead, it forms a halo at the edges of the coal particle.

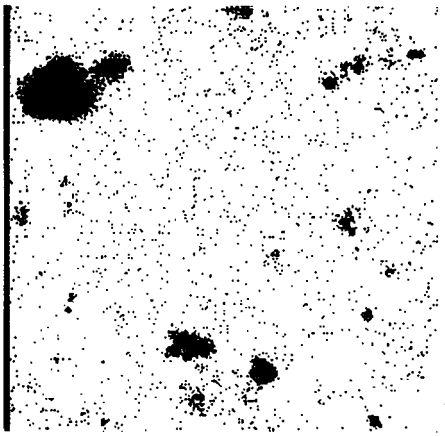

Figure 3. The EPMA micrograph is 45μm by 45μm and represents the iron distribution within the coal particle. In this image the coal particle occupies the center. The iron has not entered the particle and remains clumped outside the coal particle.

DEPTH PROFILE STUDIES OF CATALYST/ LIQUEFIED COAL RESIDUES

J.Y. Kim, P.J. Reucroft and M. Taghei
Department of Materials Science & Engineering,
University of Kentucky, Lexington, KY 40506

V.R. Pradhan and I. Wender
Chemical Petroleum Engineering Department,
University of Pittsburgh, Pittsburgh, PA 15261

INTRODUCTION

Iron based catalysts with a high specific surface area and fine particulate size can be utilized at small concentrations to achieve better performance in terms of overall coal conversion and selectivity to lighter products (oils) in direct coal liquefaction.[1] Since the surfaces of catalysts are the primary site of catalytic activity, efforts have been directed to characterizing catalyst surfaces in coal liquefaction environments. X-ray photoelectron spectroscopy (XPS) has been used to study the iron-based catalyst impregnated liquefied Blind Canyon coal residue samples at different liquefaction processing times (17, 30 and 60 minutes). It was shown that the concentration of elements at the outermost surface layer of samples measured by XPS is similar to that determined in the bulk by chemical analysis but differs from the bulk composition in some important respects.[2] In order to more carefully delineate the differences in the distribution of the elements and chemical changes between the surface and the bulk, the samples have been further analyzed by combining Ar^+ ion sputtering with XPS measurements. Special emphasis has been focused on the surface to bulk distributions of the catalytic elements iron and sulfur. The Fe peaks were not observed for most samples unless Ar^+ ion sputtering was carried out for long times. The S/Fe (catalyst element) ratio, which was initially greater than 1, decreased consistently to less than 1 as time of Ar^+ ion sputtering was increased.

EXPERIMENTAL

Three different liquefaction processing times (17, 30 and 60 min.) of iron-based catalyst impregnated Blind Canyon coal samples were investigated in the surface characterization studies. Liquefaction conversion was carried out at 400 °C with tetralin as solvent (1:1.5 coal/solvent ratio) after adding Fe_2O_3/SO_4^{2-}, so that the proportion of Fe was 5% by weight. Dimethyl disulfide was also added in amounts equivalent to Fe to promote sulfidation of the catalyst. The catalyst impregnated liquefied Blind Canyon coal residues were removed in liquid-like form after 17, 30 and 60 minutes and kept in a vacuum oven at 65 °C for 2 days to remove volatile material in the residue without exposing to an air atmosphere. The liquid-like samples were then mounted on the spectrometer probe tip by means of double-sided adhesive insulating tape. After heat treating at 65°C for 10 hours in a pretreatment chamber to remove remaining volatile materials from the coal residues, the samples were inserted into an ultrahigh vacuum chamber for surface analysis. To exclude the possibility of recording contaminants associated with the tape, the tape was also analyzed separately. It was found that the constituents of tape were not detected by XPS, and that the photoionization signals were characteristic of the samples alone.

The samples were examined by XPS employing a Kratos XSAM 800 spectrometer using Mg Kα (hν = 1253.6 eV) radiation. The spectrometer was run in Fixed Analyzer Transmission (FAT) mode at pass energy of 11 kV and 13 mA. Under these conditions, the FWHM of Ag ($3d_{5/2}$) peak is ≈ 1.0 eV. The system pressure never exceeded $3x10^{-8}$ torr during spectra acquisition. In situ Ar^+ ion sputtering of the residue samples was carried out using a differentially pumped and computor controlled 3M mini-beam ion gun. The ion beam was adjusted so that edge effects were minimized. Incident ion energy used was 3.5 kV and the sample currents were kept around 30μA (estimated etching rate was approximately 25 Angstroms/min, as determined from a SiO_2 standard film). The pressure in the main chamber was kept below $4x10^{-6}$ torr during ion sputtering. After ion sputtering, a consistent increase in the FWHM for all elements was found with increasing ion dose. No compensation was made for charging of the samples.

RESULTS AND DISCUSSION

The initially recorded XPS spectra showed a distinct peak for each of the major elements, carbon, oxygen, and silicon, as well as the minor components, sulfur and nitrogen in each sample. Binding energies of these elements showed the expected values for the most stable oxidation state and were similar to those reported previously.[2] However, Fe was not observed initially in the surface regions of the liquefied coal residue particles. A relatively high oxygen concentration was determined initially at the surface by XPS before sputtering, but a sharp drop in oxygen concentration was subsequently observed. This surface enrichment of oxygen can be ascribed to air oxidation and the oxidized layer thickness was estimated to be 50-60 nm.

Two peak components were initially observed in the case of the surface sulfur XPS signal. The peak at 168 eV, can be ascribed to oxidized sulfur, i.e., organic plus inorganic (sulfate), while the other at 163 eV corresponded to inorganic sulfide plus the usual organic sulfur forms present in coal (thiophene, sulfides, mercaptans). As sputtering increased, the sulfate peak decreased and finally disappeared, while the sulfide peak showed an increase in intensity. This observation is in agreement with the decrease of oxygen concentration which was observed as the sputtering increased. These results are similar to those reported previously.[2]

The Fe peaks were not observed initially for most samples unless ion sputtering was carried out for at least 30 minutes. As the liquefaction reaction time increased from 17 to 60 min, sputtering time had to be further increased in order to observe the Fe peaks. Catalytic elements such as iron and sulfur showed a systematic trend towards higher concentrations of each sample after 30 min Ar^+ sputtering. The results are shown in Figures 1, 2, and 3. From these results, it can be concluded that the iron catalyst particles are well encapsulated in either oxide layers or within other organic materials from the coal residues.

The S/Fe (catalyst element) ratio, which was initially greater than 1, decreased consistently to less than 1 as time of Ar^+ ion sputtering was increased (Tables 1, 2 and 3). This is also shown in Figures 1, 2 and 3 for liquefaction times of 17, 30 and 60 minutes, respectively. EXAFS and Mossbauer studies have shown that under the liquefaction conditions that were employed i.e., after adding dimethyl disulfide to the catalyst/coal residue mixtures, the ion catalyst is converted to iron sulfide (pyrrhotite) within a few minutes of starting the reaction.[3] Further analysis is currently underway.

SUMMARY AND CONCLUSIONS

Surface analysis combined with depth profiling shows that the sulfur/iron stoichiometry varies in iron catalyst/liquefied coal residues that have been extracted from coal liquefaction environments. The catalyst elements become increasingly more encapsulated in the carbonaceous material as the processing time increases. The S/Fe atomic ratio approaches 0.7 to 0.9 inside the coal residue particles.

ACKNOWLEDGEMENT

We gratefully acknowledge financial support from the Consortium for Fossil Fuel Liquefaction Science, University of Kentucky under Dept. of Energy Contract No. DE-FC22-92 PC 90029. We also thank Dr. G.P. Huffman for his interest in this work.

REFERENCES

1. F.J. Derbyshire, Catalyst in Coal Liquefaction: New Direction for Research , IEA Coal Research: London, 1988; IEA CR-08.

2. J.Y. Kim, P.J. Reucroft, V.R. Pradhan and l. Wender, American Chem. Soc., Div. of Fuel Chem. Preprints, **37**, 756 (1992); to be published in Fuel Processing Technology.

3. M. Taghei, Private Communication.

Table 1. XPS Catalyst Element Depth Profile for Ar^+ Sputtered 17 min Liquefied Coal Residues (atomic %)

	0 min	10 min	20 min	30 min	40 min	50 min	60 min
S	0.38	0.48	0.76	0.50	0.58	0.73	0.89
Fe	-	-	-	0.40	0.73	0.89	1.24
S/Fe	-	-	-	1.25	0.79	0.82	0.72

Table 2. XPS Catalyst Element Depth Profile for Ar^+ Sputtered 30 min Liquefied Coal Residues (atomic %)

	0 min	10 min	20 min	30 min	40 min	50 min	60 min
S	0.25	0.23	0.34	0.43	0.51	0.72	0.97
Fe	-	-	-	0.20	0.45	0.69	1.12
S/Fe	-	-	-	2.15	1.13	1.04	0.87

Table 3. XPS Catalyst Element Depth Profile for Ar^+ Sputtered 60 min Liquefied Coal Residues (atomic %)

	0 min	10 min	20 min	30 min	40 min	50 min	60 min
S	0.62	0.53	0.42	0.38	0.37	0.62	0.63
Fe	-	-	-	0.17	0.23	0.52	0.74
S/Fe	-	-	-	2.24	1.61	1.19	0.85

Figure 1. Depth Profile of Elements for 17 min. Coal Liquefaction Residue

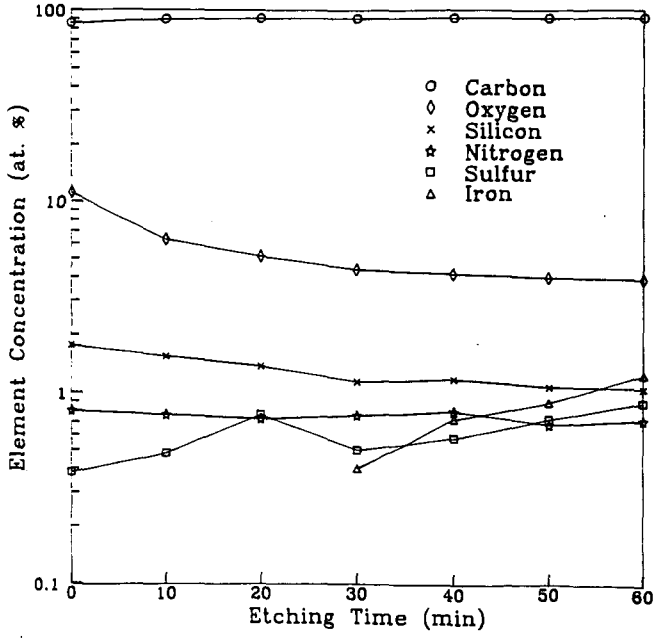

Figure 2. Depth Profile of Elements for 30 min. Coal Liquefaction Residue

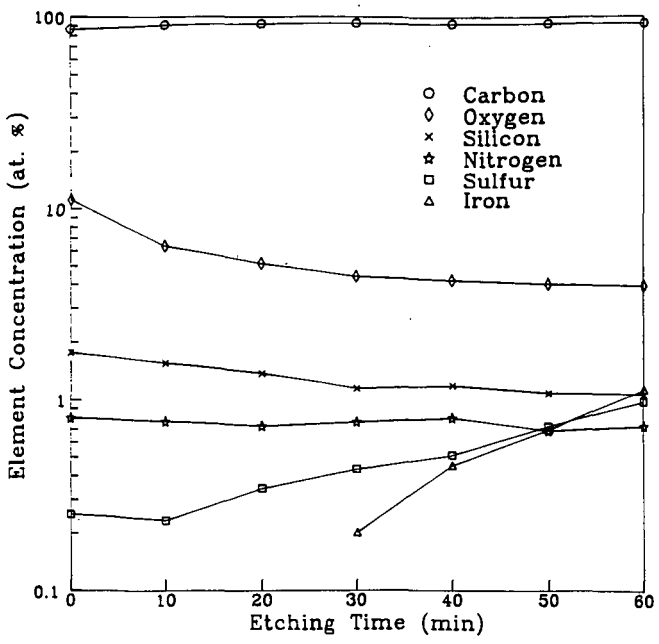

Figure 3. Depth Profile of Elements for 60 min. Coal Liquefaction Residue

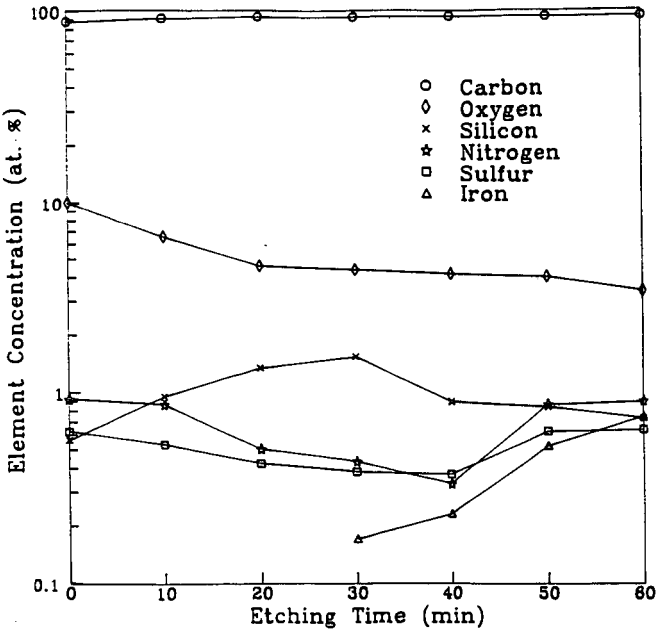

ACTIVITY TESTING OF FINE-PARTICLE SIZE, UNSUPPORTED, IRON-BASED CATALYSTS*

Frances V. Stohl
Process Research Department 6212
Sandia National Laboratories
P.O. Box 5800
Albuquerque, NM 87185

Keywords: Fine-particle catalysts; activity testing; statistical design

INTRODUCTION

The efficiency of the initial reactions of coal during coal liquefaction will have significant impacts on downstream processing (including catalyst usage, reaction severity, product yields, product quality) and hence on process economics. Reactions that result in compounds with low molecular weights and decreased boiling points are beneficial, whereas retrogressive reactions, which yield higher molecular weight compounds that are refractory to further processing, decrease process efficiency. Likewise, reactions that result in decreased sulfur, nitrogen, and oxygen contents and increased hydrogen contents in the products are beneficial. The use of unsupported fine-particle (<40 nm) catalysts during initial coal processing has the potential to enhance desired reactions and minimize retrogressive reactions. The potential advantages of using fine-particle size catalysts include improved dispersion of the catalyst, improved coal/catalyst contact, and the potential for using low amounts ($\leq$0.5% based on the weight of coal) of these novel catalysts due to their very high surface areas. These catalysts could be combined with the coal or coal-solvent mixture as either active catalysts or catalyst precursors that would be activated in situ. Several methods of combining catalyst and coal, such as physical mixing or using a catalyst-hydrogen donor slurry, are possible. Ideally the fine-particle catalysts would be inexpensive enough to be disposable.

The Pittsburgh Energy Technology Center's (PETC) Advanced Research (AR) Coal Liquefaction Program has many research projects to develop fine-particle size catalysts that are active for reactions of interest in direct coal liquefaction: hydrogenation, carbon-carbon bond breakage, and heteroatom removal. However, it is difficult to compare results among researchers because of the variety of testing procedures used including different reactors, reaction temperatures, reaction times, pressures, hydrogen donor solvents, solvent to coal ratios, and workup procedures. In addition, some catalyst developers in the AR program do not have any testing capabilities for direct liquefaction. The objectives of the work reported here are to develop standard coal liquefaction test procedures and to perform the testing of the novel fine-particle size catalysts being developed in the PETC AR Coal Liquefaction Program.

EXPERIMENTAL PROCEDURES

Materials

The coal being used in this project is the DECS-17 Blind Canyon Coal obtained from The Penn State Coal Sample Bank. The coal, which is packaged under an

* This work was supported by the U. S. Department of Energy at Sandia National Laboratories under contract DE-AC04-76DP00789.

inert atmosphere in sealed foil bags with a plastic liner, is stored in a refrigerator prior to use. The coal is a HVA bituminous coal with 0.36% iron, 0.02% pyritic sulfur, and 7.34% mineral matter (on a dry basis). The particle size is -60 mesh. The coal is riffled three times with remixing prior to taking splits. 1,2,3,6,7,8-hexahydropyrene (H_6Py) and 9,10-dihydrophenanthrene (DHP) were evaluated as hydrogen donors for use in the standard tests. H_6Py was obtained from Aldrich (98% purity), and DHP was obtained from either Aldrich (94% purity) or Janssen Chimica (97% purity). Pyrite (99.9% pure on a metals basis) with a -100 mesh particle size was obtained from Johnson-Matthey. An X-ray diffraction pattern taken on this material showed only pyrite. The surface area of the pyrite is 0.7 m^2/g as measured using BET techniques. Stabilized tetrahydrofuran (THF) and heptane are used in product workups.

Reactors

The testing is being performed using batch microautoclaves consisting of a 0.75" OD Swagelok "T" connected to 0.375" OD high pressure stainless steel tubing. A Whitey plug valve at the top of the tubing is used for pressurizing and depressurizing the reactors. A thermocouple was inserted into the reactor, and a pressure transducer was attached. The total volume for a reactor is 43 cm^3 with a liquid capacity of up to 8 cm^3. Four reactions can be run simultaneously. After being charged with the reactants (coal, hydrogen donor solvent, high pressure gas, and other additives required by the experimental design such as catalyst or sulfur), the reactors are rapidly heated to temperature in a fluidized-sand bath while being agitated at 200 cycles/sec with a wrist-action shaker. Temperatures and pressures are recorded with a digital data acquisition system during the course of the experiments. Following the heating period, the reactors are rapidly quenched in a water bath to ambient temperature, a gas sample is taken, and the liquid and solid products are removed for analysis.

Product Analyses

The primary criteria for evaluating catalysts are based on coal conversion. Reaction product analyses that are performed routinely include THF and heptane solvent solubility determinations, gas chromatographic (GC) analyses of the hydrogen donor, and analyses of gas products. Solvent solubilities are done using pressure filtration procedures with a Millipore 142 mm diameter pressure filtration device and Duropore (0.45 micron) filter paper. Quantitative GC analyses using methylnaphthalene as an internal standard are performed on the THF soluble material to determine the recovery of the hydrogen donor and the amounts of both DHP and phenanthrene present in the product. The quantity of each gas in the product is calculated using the ideal gas law, the mole percent in the gas sample as determined from a Carle GC using standard gas mixtures, and the post-reaction vessel temperature and pressure.

RESULTS AND DISCUSSION

Two important aspects of the catalyst testing program are the development of standard test procedures and the development of a statistical experimental design.

Standard Test Procedures

The standard test procedures cover both performing the reactions and doing product workups. H_6Py and DHP were evaluated for use as hydrogen donors in the standard tests. DHP was chosen because it is less expensive than H_6Py and has a lower melting point (32-35°C) that could help ensure good mixing. It also performed well in experiments. Current coal liquefaction processing

configurations use approximately a 2:1 hydrogen donor solvent to coal ratio. In addition, some of the better recycle solvents from large-scale processes contain about 1% donatable H_2, which is considered very good. Use of DHP at a 2:1 donor solvent:coal ratio gives about 1% donatable hydrogen and a high liquid:coal ratio for aiding catalyst dispersion.

Procedures have been set up to obtain excellent temperature control during the course of the reactions. The average temperature is routinely within one degree of the desired temperature and the standard deviation is <1°C. Heat-up times are about 3.5 minutes for 400°C reactions and quench times to temperatures <50°C are about 2 minutes.

After the gas samples are collected, the reactors are opened and the Swagelok tees and end caps containing the product are sonicated in THF, soaked in THF overnight, and then sonicated again prior to filtration. The total time the liquid products are in THF is about 17 hours. The volume of THF used in this reactor cleaning is 200 ml. Typically, three filter papers are used for THF filtration. The filter cake is rinsed with THF prior to opening the device. After the filtration is complete, the filter paper is dried in a vacuum oven, cooled to room temperature and weighed to determine the insoluble portion. The THF solubles are then rotoevaporated to about 50 to 60 ml volume, quantitatively transferred to a 100 ml volumetric flask and brought to 100 ml volume after the solubles have cooled to room temperature. A 1 ml portion is removed and used for determination by GC of the hydrogen donor recovery, including both DHP and phenanthrene. The remaining 99 ml is rotoevaporated until there is no weight loss after 10 minutes of rotoevaporating. A stirring bar is added to the flask and 200 ml heptane is added with constant stirring. This heptane/product mixture is then pressure filtered to obtain the weight of heptane insolubles.

Statistical Experimental Design

There are two main reasons for using an experimental design: to enable good comparisons among novel catalysts and to obtain more information with fewer experiments. This procedure will give statistical information regarding the results and will yield optimum processing conditions for each catalyst over the ranges of the variables studied. The statistical experimental design (Figure 1) that was chosen evaluates the effects of three variables: time (20 to 60 minutes), temperature (350 to 400°C) and catalyst loading (0 to 1 wt% on a weight of as-received coal basis). These conditions are consistent with process conditions used in coal liquefaction. An additional advantage of using an experimental design is that the impacts of additives, such as sulfur required to activate an Fe_2O_3 catalyst, can be easily evaluated by adding sulfur to the thermal baseline reactions.

Evaluation of the Statistical Design

This experimental design was evaluated by each of two operators using pyrite. Pyrite was chosen because it is a known iron catalyst in coal liquefaction, is commercially available, and is easy to work with.

The hydrogen donor recoveries (including both DHP and phenanthrene) were greater than 90% for all the reactions. At the lower severity conditions about 83% of the donor product was DHP, whereas at the higher severity conditions only 24% was DHP. The non-hydrogen gases detected in the reaction products were CO_2, CO, CH_4, and C_2H_6. The quantities of these gases produced ranged from 0.23% (dmmf coal basis) for the lowest severity conditions to 2.21% for the highest severity conditions. Table 1 shows the measured, gas

corrected THF conversions and heptane conversions obtained by each operator for the nine sets of process conditions in the experimental design. It also gives the average conversions and the standard deviations. The THF results show good reproducibility. The largest standard deviation is 4.09 for the center point of the cube. This high value is consistent with the fact that both operators indicated the products from runs made at these conditions are the most difficult to filter. The equation obtained by fitting the THF conversion data to a linear model is as follows:

THF Conv(%) = 70.908+(+/-)16.938+(+/-)6.931+(+/-)1.091+(+/-)(+/-)(-1.956)

Where:

70.908	Center Point Conversion
16.938	Temperature Effect
6.931	Time Effect
1.091	Pyrite Effect
-1.956	Time x Temperature Interaction

The r^2 value for the fit of the THF data to this equation is 0.987. To calculate the THF conversion for a given set of reaction conditions choose either the + or - in each (+/-). Use + for each high value: 400°C or 60 minutes or 1 wt% catalyst. Use - for each low value: 350°C or 20 minutes or no catalyst. This analysis shows that the largest effect is due to temperature, followed by time and finally pyrite addition. There is also some interaction between temperature and time. No other interactions were observed. The calculated THF values for the points on the cube are shown in Figure 2. The results show that the impact of a 1% pyrite addition is to increase the THF conversion by 2.2%, which is a statistically significant increase. It also shows that the effect is the same at both the lowest and highest severity conditions.

The measured heptane conversions in Table 1 show much greater variability than the THF conversions. Approximately halfway through the experimental design, it was observed that there was a systematic difference between the heptane conversion values obtained by the two operators. Therefore, the procedure was revised to ensure that both operators were doing the workups the same way. The results for the runs that were made after this change are indicated with an "*". A comparison of the results from the revised procedure to those from the old procedure shows significant improvement in reproducibility. All of the measured heptane conversions were used in the linear modeling effort because there would not be enough data if the old workup procedure results were discarded. The equation obtained by fitting the heptane conversion data to a linear model is as follows:

Heptane Conv(%) = 19.958+(+/-)13.020+(+/-)5.255+(+/-)(+/-)2.406

Where:

19.958	Center Point Conversion
13.020	Temperature Effect
5.255	Time Effect
2.406	Time x Temperature Interaction

The r^2 value for the fit of the heptane conversion data to this equation is 0.957. The calculated heptane values are shown in Figure 3. This analysis indicates that the largest effect is due to temperature, followed by time. Pyrite addition had no effect on heptane conversion. There is also an

interaction between temperature and time. No other interactions were observed. The estimates of standard errors associated with this data could probably be improved by repeating the experimental design using the new workup procedure for all experiments. This might show somewhat different results. The heptane conversion (4.09%) for 350°C for 20 minutes is equal to that obtained from the as-received coal.

Operator effects were also analyzed as part of the statistical analysis of the results. Operator effects include both effects between operators and within each operator. The results were as follows:

	ESTIMATES OF STANDARD DEVIATION	
SOURCE	THF CONVERSIONS	HEPTANE CONVERSIONS
Between Operators	0.23	0.31
Within Operators	1.78	0.95

These results show good reproducibility both between operators and within each operator and thus indicate that there are no systematic differences in the procedures used by the operators. Only the results from the new workup procedure were used in this analysis of the heptane conversions.

SUMMARY

The results of the experiments performed using pyrite have shown that small differences in activity can be detected by using a statistical experimental design. The differences in THF conversion were 2.2% between thermal and catalytic reactions. This difference was unaffected by changes in reaction time and temperature over the parameter ranges used in this study. The results also show that the experimental procedures (with the revised heptane conversion techniques) can be well duplicated between operators and within a single operator.

FUTURE WORK

Future work will include repeating the statistical experimental design to determine if the revised heptane procedure impacts the conclusions. The hydrogen donor to coal ratio will also be varied to determine the effects on catalyst activity. Efforts will be made to develop a procedure for obtaining information on the quality of the reaction products by performing elemental analyses on the THF and heptane insoluble materials. Testing of a novel catalyst being developed by I. Wender at the University of Pittsburgh will be initiated. This will be the first novel catalyst that will be evaluated using this experimental design.

Acknowledgement
I would like to express my thanks to Jeff Kawola and Richard Jensen for performing the experimental work associated with this project. I would also like to thank Kathleen Diegert for determining the best experimental design and analyzing the results and Carlos Quintana for his efforts in setting up the new testing facility.

TABLE 1. MEASURED CONVERSIONS

TEMP (°C)	TIME (min)	CAT (wt%)	THF RESULTS OPERATOR #1	#2	AVERAGE	STD DEV	HEPTANE RESULTS OPERATOR #1	#2	AVERAGE	STD DEV
350	20	0	42.5	44.0	43.2	1.05	3.0	6.6	4.8	2.55
400	20	0	82.2	79.2	80.7	2.16	25.6*	25.1*	25.3	0.33
350	60	0	61.4	60.9	61.1	0.34	6.6	13.0	9.8	4.53
400	60	0	93.0	91.6	92.3	0.72	37.8	48.4	42.1	4.58
			91.7				39.9*			
			92.9				42.5*			
375	40	0.5	74.6	74.9	71.8	4.09	15.7	22.2	17.2	3.07
			65.1				17.6*			
			70.6	73.7			14.1*	16.4*		
350	20	1	47.2	45.9	46.1	1.20	2.4	3.9	4.6	2.05
			44.5	46.9			4.9*	7.3*		
400	20	1	84.0	83.9	83.9	0.03	26.7*	27.4*	27.0	0.45
350	60	1	62.1	64.9	63.5	2.02	11.3*	11.7*	11.5	0.26
400	60	1	93.2	92.6	92.8	0.28	35.0	40.4	40.0	3.53
			92.7	92.7			41.9*	42.9*		

* = Revised work up procedure

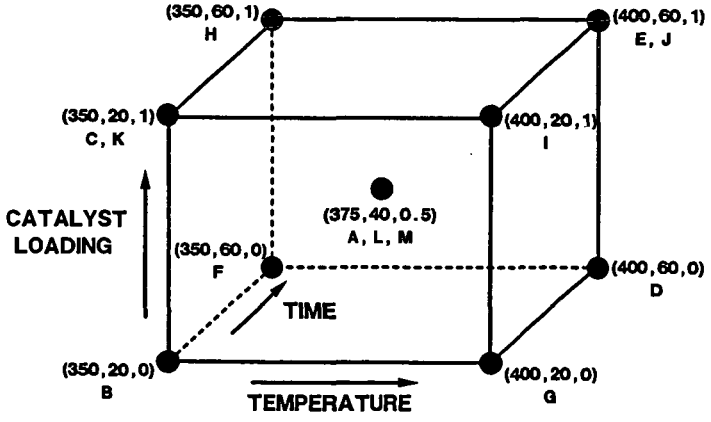

(TEMPERATURE = °C; TIME = MINUTES; CATALYST LOADING = WT % AR COAL)
LETTERS = ORDER IN WHICH REACTIONS WERE PERFORMED

Figure 1: Statistical experimental design

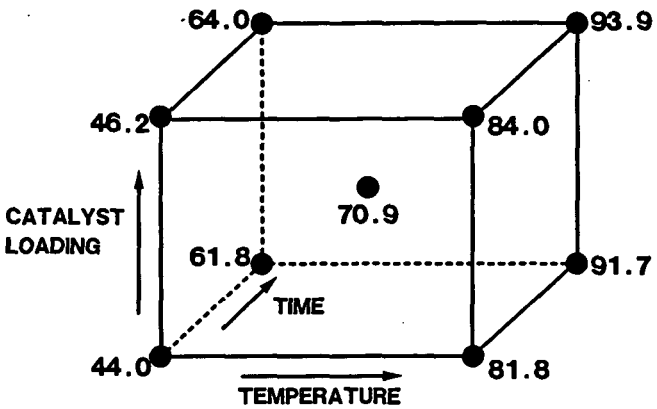

(TEMPERATURE = °C; TIME = MINUTES; CATALYST LOADING = WT % AR COAL

Figure 2. THF conversions: Calculated from the linear model

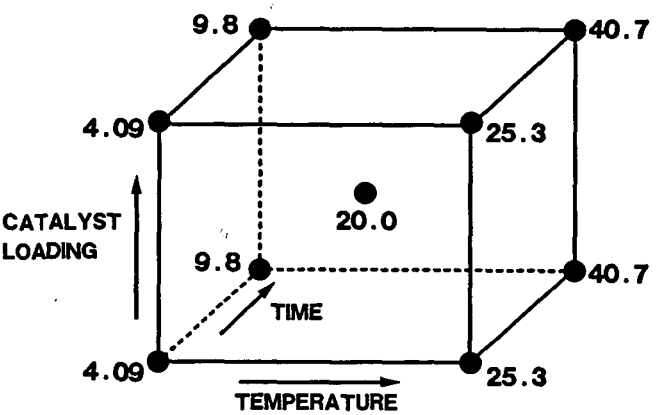

(TEMPERATURE = °C; TIME = MINUTES; CATALYST LOADING = WT % AR COAL

Figure 3. Heptane conversions: Calculated from the linear model

THE EFFECT OF CO COADSORPTION ON THE HYDROGENATION PROPERTIES OF IRON

R. T. K. Baker, M. S. Kim and N. M. Rodriguez
Materials Research Laboratory
The Pennsylvania State University
University Park, PA, 16802

Keywords: Iron catalysts, hydrogenation catalysts, ethylene decomposition

ABSTRACT

During the course of a series of reactions designed to examine the differences in carbon deposition characteristics exhibited by CO and C_2H_4 over iron an unexpected pattern of behavior was found. Exposure of the metal to a C_2H_4-H_2 mixture at 600°C resulted in only minor decomposition of the olefin, however, upon addition of a small amount of CO to the system, there was a dramatic increase in the amount of filamentous carbon formed, of which the major fraction could be attributed to decomposition of C_2H_4. Maximum reactivity was achieved with a C_2H_4-CO-H_2 (3:1:1) mixture and it was apparent that CO was responsible for not only promoting the formation of solid carbon, but also inducing the conversion of C_2H_4 to C_2H_6. Removal of CO from the system resulted in a rapid decline in catalytic activity, however, upon re-introduction of CO activity was restored to its initial high level, indicating that the reversible nature of the activation-deactivation processes. This behavior is rationalized in terms of a reconstruction of the iron surface in the presence of coadsorbed CO which results in the possible formation of various faces with differing reactivity characteristics, and a relaxation when CO is removed from the reactant.

INTRODUCTION

The high activity of iron with CO has only been observed when some additive gas such as hydrogen, water vapor or other oxygenates were mixed with the reactant [1-3]. Dry and coworkers [2] reported that in all the cases where enhancement of carbon deposition was observed then hydrogen was shown to be present within the catalyst bed. They suggested that the increase in solid carbon formation was related to the ability of hydrogen to strengthen the adsorption characteristics of CO to the iron and as a consequence increase its rate of decomposition.

It is known that disproportionation of CO takes place via the Boudouard equilibrium,

$$2CO \longrightarrow C + CO_2 \qquad \{1\}$$

which favors the right side at temperatures below 700°C. The promotional effects of hydrogen on the decomposition of CO have been interpreted in two ways. The first, the occurrence of a secondary reaction (CO hydrogenation) to produce solid carbon [1,3]:

$$CO + H_2 \longrightarrow C + H_2O \qquad \{2\}$$

In addition to this process, hydrogen adsorbed on the metal surface was also found to catalyze the Boudouard reaction and this effect has been explained by the ability of hydrogen to decompose inactive metal carbides into the catalytically active metallic phase [1]. There have been numerous investigations which have dealt with the interaction of CO and hydrogen on transition metal surfaces and these have been comprehensibly reviewed by Vannice [4]. It is generally agreed that the uptakes of CO and hydrogen are mutually enhanced by a coadsorption procedure compared to that of either gas alone and this aspect was rationalized in terms of the formation of a surface complex between the two adsorbate molecules.

Perhaps the clearest understanding of the interaction of CO-H2 with iron comes from recent surface science studies performed by Madix and coworkers [5,6] of the coadsorption of CO and H2 on Fe(100) surfaces. It was suggested that adsorbed CO induced a weakening in the strength of the Fe-H bond, which triggered the formation of a potentially more reactive hydrogen species. In a subsequent investigation Burke and Madix [7] demonstrated the validity of this argument in experiments where the introduction of CO onto an iron surface pre-saturated with hydrogen brought about the formation of ethane from coadsorbed ethylene, a reaction which did not occur in the absence of CO [8].

The current investigation was undertaken in an attempt to gain a fundamental understanding of the differences in the reactivity of ethylene-hydrogen mixtures both in the absence and presence of carbon monoxide, when passed over an iron catalyst.

EXPERIMENTAL

The experiments reported here were carried out in a flow reactor system operated at 1 atm total pressure. There was provision for taking samples at various intervals during reaction for gas product analysis by gas chromatography. Powdered iron catalyst samples (50 mg) were held in a ceramic boat which was placed at the center of the reactor tube. After reduction of the sample in a 10% H2-He mixture for 2 hours at 600°C, the system was flushed with helium and then the reactant, either pure CO, CO-H2, C2H4-H2 or CO-C2H4-H2 mixtures, was introduced into the system and allowed to react with the iron catalyst at 600°C for periods of up to 5 hours. The total amount of carbon deposited during the experiment was determined by weight difference. The composition of the gas phase was monitored as a function of time from analysis performed in a Varian 3400 GC equipped with a 30 m megabore column (GS-Q). Iron powder (200 mesh) was obtained from Johnson Matthey Inc. (99.99% purity) and had a BET nitrogen surface area of 0.3 m^2/g^{-1} at -196°C.. The gases used in this work CO (99.9%), hydrogen (99.999%), ethylene (99.99%) and helium (99.99%) were obtained from Alphagaz company and used without further purification.

RESULTS AND DISCUSSION

Iron Catalyzed Decomposition of C2H4-H2 and CO-C2H4-H2 Mixtures

When C2H4-H2 (3:1) mixture was passed over iron at 600°C, the reactivity of the system was very low, only about 0.43% of solid carbon being produced with no detectable amounts of other products being formed. This is consistent with the notion that iron is not a very active hydrogenation catalyst in its pure form [8]. After a period of about 1 hour, CO was introduced into the feed gas in sufficient concentration to create a CO-C2H4-H2 (1:3:1) mixture. The addition of CO to the reactant resulted in a dramatic increase in the percent of ethylene undergoing reaction, rising from 0.51 to 79.7%, over a 30 min period of time. It appears that the presence of CO induces changes in the surface of the iron catalyst which enhances its ability to adsorb and decompose ethylene.

In a further series of experiments, initially a CO-C2H4-H2 (1:3:1) mixture was passed over an iron catalyst, and the same high levels of ethylene decomposition as those produced in the previous experiment were obtained. After 80 minutes reaction time, the CO flow was stopped and this action resulted in a dramatic decrease to around 0.5 %, a level comparable to that obtained with a C2H4-H2 (3:1) mixture in the previous experiment. When the CO flow was re-introduced into the feed 45 minutes later, the percentage of ethylene undergoing reaction was restored to the original high level. This sequence of events indicates that the catalyst activation-deactivation process is reversible and the high olefin decomposition activity occurs only when CO is present in the reactant mixture.

In order to investigate the details of the influence of CO on the decomposition of ethylene, the ratio of CO in CO-C_2H_4-H_2 mixtures was varied from 0 to 1 (CO fraction = CO/{CO+C_2. The gaseous product distribution obtained with the various mixtures are presented in Table 1. Since the amount of methane produced was relatively small and that produced from CO was negligible with the feed containing a small portion of hydrogen, the error resulting from the approach should not be appreciable. Inspection of this data shows that coadsorption of CO on the iron catalyst not only promotes the formation of ethane via the hydrogenation step, but also has a tremendous impact on the fate of the carbon species produced on the metal surface from the C-C bond cleavage of the adsorbed ethylene molecules. It is known from previous studies [8] that in the absence of CO, ethylene adsorbs reversibly without dissociation on hydrogen pre-saturated iron surfaces and it is therefore not surprising to find that very little solid carbon is produced on the metal. In the presence of CO, the metal is activated towards ethylene decomposition and the carbon species formed at the surface proceed to dissolve into the bulk of the particle and eventual precipitation at the rear faces in the form of a filament. This is obviously a facile process since filamentous carbon is formed in abundance and its growth is sustained for relatively long periods of time.

When CO is removed from the reactant then the fraction of ethylene which decomposes declines to the level exhibited by the CO-free iron surface. On re-introduction of CO the amount of ethylene which is decomposed is quickly restored to a high level demonstrating the reversible nature of the promotional effect. It is possible that adsorption of CO induces reconstruction of the surface to a configuration which facilitates rupture of the C=C bond in ethylene. Elimination of CO from the system causes a relaxation of the reconstructed surface to a structure which no longer favors ethylene decomposition. It is also worth taking into consideration the possibility that the presence of CO produces electron perturbations which alter the bonding characteristics between the ethylene and metal surface atoms.

It is interesting to compare the relative amounts of methane formed in the present system with that produced from the decomposition of C_2H_4-H_2 mixtures over copper-nickel alloy particles [9] where over 20% of the ethylene decomposed to form methane. The excessive amount of methane generated in this latter system was purported to result from the formation of an "ethylidyne" intermediate. It would appear, therefore, that in the present system, where the methane yield under comparable conditions is less than 1%, the formation of an "ethylidyne" intermediate is not a favored step.

From a consideration of the product distribution it is possible to make certain speculations regarding the mode by which which ethylene is adsorbed on the iron surface containing coadsorbed CO and H_2. The formation of a relatively large amount of ethane from the CO-induced hydrogenation of the olefin suggests that there is a strong tendency for the ethylene molecules to bind in an arrangement in which the C=C bond is "parallel" to the metal surface, as depicted in Figure 1a. Conversely, the low amount of methane produced during this reaction indicates that there is a reluctance for ethylene to adsorb in the "end-on" configuration, where one of the carbon atoms in the molecule is attached to three metal atoms in the form of an "ethylidyne" conformation, as illustrated in Figure 1b.

CONCLUSIONS

In the present investigation ethylene was used as a model hydrogen acceptor molecule. It was found that iron exhibited very little activity for the hydrogenation of the olefin, however, when as little as 7% CO was added to the hydrocarbon-hydrogen mixture, the hydrogenation activity of the metal was substantially enhanced. Such an increase in hydrogenation activity was observed over a wide range of temperature, however, at 600°C one has to contend with the concomitant formation of a large amount of solid carbon. The presence of coadsorbed CO induces a weakening in the strength of the metal-hydrogen bond, which gives rise to the formation of a very reactive hydrogen species. These model studies demonstrate that the introduction of a gas additive, such as CO, into the reactant stream can effectively convert a metal which in its pure state is relatively inert into an

extremely active hydrogenation catalyst, and we believe that this concept could be extended to hydrogenation of coal and its derivatives.

ACKNOWLEDGMENTS

Support for this work was provided by the National Science Foundation, under Grant CBT-8800931.

REFERENCES

1. Walker, Jr., P. L., Rakszaski, J. F., and Imperial, G. R., J. Phys. Chem. 63, 140 (1959).
2. Dry, M. E., Shingles, T., Boschoff, L. J., and Van H. Botha, C. S., J. Catal. 17 347 (1970).
3. Turkdogan, E. T. and Vinters, J. V., Met. Trans. 5, 11, 21, (1974).
4. Vannice, M. A., in "Catalysis Science and Technology" Vol. 3 (J. R. Anderson and M. Boudart ed.), Springer-Verlag, New York, 1982, p. 139.
5. Benziger, J. B., and Madix, R. J., Surf. Sci. 115, 279 (1982).
6. Burke, M. L. and Madix, R. J., Surf. Sci. 237, 20 (1990).
7. Burke, M. L. and Madix, R. J., J. Am. Chem. Soc. 113, 1475 (1991)
8. Burke, M. L. and Madix, R. J., J. Am. Chem. Soc. 113, 3675 (1991).
9. Kim, M. S., Rodriguez, N. M., and Baker, R. T. K., J. Catal. 131, 60 (1991).

TABLE 1. EFFECT OF GAS COMPOSITION ON THE GASEOUS PRODUCT DISTRIBUTION FORM THE INTERACTION OF C_2H_4-CO-H_2 MIXTURES OVER IRON AFTER 60 MINUTES AT 600°C

C_2H_4:CO:H_2	% C_2H_4 Decomposition	% CH_4 formed	C_2H_6 formed
80: 0 :20	0.51	-	-
73: 7 :20	29.53	0.73	8.5
68:12:20	60.28	0.58	9.4
60:20:20	79.47	1.07	10.3
38:42:20	76.10	2.7	5.5
17:63:20	54.30	2.6	5.8
0 :80:20	21.95	0.05	--

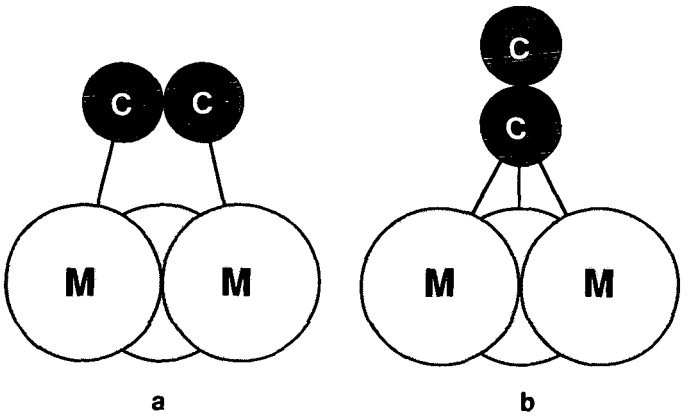

FIGURE 1.STRUCTURAL ARRANGEMENT FOR (a) ETHYLENE BONDED PARALLEL TO METAL SURFACE AND (b) ETHYLENE BONDED TO METAL IN THE STABLE "ETHYLIDYNE" CONFORMATION